J. Fluid Mech. (1994), *vol.* 264, *pp.* 343–372

Interaction of oblique instability waves with a nonlinear plane wave

By DAVID W. WUNDROW[1], LENNART S. HULTGREN[2] AND M. E. GOLDSTEIN[2]

[1]Sverdrup Technology, Inc., Lewis Research Center Group, Cleveland, OH 44135, USA

[2]National Aeronautics and Space Administration, Lewis Research Center, Cleveland, OH 44135, USA

(Received 25 March 1993 and in revised form 7 October 1993)

This paper is concerned with the downstream evolution of a resonant triad of initially non-interacting linear instability waves in a boundary layer with a weak adverse pressure gradient. The triad consists of a two-dimensional fundamental mode and a pair of equal-amplitude oblique modes that form a subharmonic standing wave in the spanwise direction. The growth rates are small and there is a well-defined common critical layer for these waves. As in Goldstein & Lee (1992), the wave interaction takes place entirely within this critical layer and is initially of the parametric-resonance type. This enhances the spatial growth rate of the subharmonic but does not affect that of the fundamental. However, in contrast to Goldstein & Lee (1992), the initial subharmonic amplitude is assumed to be small enough so that the fundamental can become nonlinear within its own critical layer before it is affected by the subharmonic. The subharmonic evolution is then dominated by the parametric-resonance effects and occurs on a much shorter streamwise scale than that of the fundamental. The subharmonic amplitude continues to increase during this parametric-resonance stage – even as the growth rate of the fundamental approaches zero – and the subharmonic eventually becomes large enough to influence the fundamental which causes both waves to evolve on the same shorter streamwise scale.

1. Introduction

Boundary-layer transition experiments often involve controlled forcing of the unsteady flow by relatively two-dimensional single-frequency excitation devices such as vibrating ribbons, heating strips, or acoustic speakers. The resulting initial disturbances are nearly two-dimensional and well described by spatially growing linear instability modes. This behaviour can persist over long streamwise distances when the excitation levels are sufficiently small, but three-dimensional effects eventually come into play, as evidenced by the appearance of Λ-shaped structures in flow-visualization experiments. These structures can either be aligned or staggered in alternating rows.

The aligned arrangement is commonly referred to as 'peak–valley' splitting and was originally observed by Klebanoff, Tidstrom & Sargent (1962). The staggered arrangement, which usually appears at lower excitation levels, is now believed to be the result of a resonant-triad interaction between a pair of oblique subharmonic modes (which originate from the background disturbance environment) and the

two-dimensional fundamental mode. The significance of this type of interaction was originally realized by Raetz (1959) and subsequently analysed for viscosity-dominated Tollmien–Schlichting-type instabilities by Craik (1971), Mankbadi, Wu & Lee (1993), and many others. Craik (1971) also proposed that the aligned (or Klebanoff) arrangement could result from a resonant-triad interaction between a pair of oblique modes at the forcing frequency and the small two-dimensional instability mode that is invariably generated at the first harmonic of this frequency (see §5.2 of Kachanov & Levchenko 1984 for a more complete discussion of this issue). All of the relevant modes can then be generated by the excitation device and do not have to emanate from the background disturbance environment. However, the observed gradual transition from a two- to a three-dimensional flow structure can only occur if the (common) amplitude of the oblique modes is able to exceed that of the (small) two-dimensional first harmonic that is the cause of the enhanced growth in the Craik (1971) model. This behaviour would obviously be favoured if the oblique modes were unable to suppress the growth of the first harmonic until they themselves become very large. This allows the oblique modes to continue their super-exponential growth until they become larger than the more slowly growing two-dimensional fundamental mode.

Since transition in technological devices usually occurs in regions of decelerating flow, Goldstein & Lee (1992, hereinafter referred to as G&L) analysed the resonant-triad interaction between two equal-amplitude oblique modes (which form a standing wave in the spanwise direction) and a single two-dimensional mode in a boundary-layer flow with a relatively weak adverse pressure gradient. The wavelengths in their analysis are therefore large, $\propto$ (pressure gradient)$^{-\frac{1}{2}}$, and the corresponding growth rates are small, $\propto$ (pressure gradient)^2. The relevant waves have a well-defined common critical layer, which turns out to be of the non-equilibrium (or growth-dominated) type rather than the equilibrium (or viscosity-dominated) type associated with Tollmien–Schlichting waves. The G&L analysis, which applies to both the subharmonic and peak–valley transition processes, shows that the first interaction between the initially linear spatially growing waves takes place within this common critical layer and results in an enhanced oblique-mode growth rate due to a parametric-resonance (or secondary) instability of the nearly periodic motion produced by the basic boundary-layer flow and the plane wave. G&L also show that the oblique modes do not affect the plane wave until the ratio of their common amplitude to that of the latter becomes $\propto$ (pressure gradient)$^{-\frac{3}{2}}$, which supports Craik's (1971) contention that the peak–valley transition processes is due to a resonant triad interaction. G&L go on to show that the parametric-resonance stage is followed by a fully coupled stage which always ends in a singularity at a finite downstream position in the inviscid limit.

In contrast to the situation considered by G&L where the plane wave is completely linear in the parametric-resonance stage, the present investigation is concerned with the case where the common amplitude of oblique modes is small enough at the start of the parametric-resonance stage so that the plane wave becomes nonlinear before being affected by the oblique modes. The nonlinearity occurs within the plane-wave critical layer and causes a reduction of the growth rate of this wave. This behaviour is particularly relevant to the subharmonic transition process since it is most likely to occur when the initial common amplitude of the oblique modes is small compared to that of the plane wave.

This paper is organized as follows. The problem is formulated in §2, where it is shown how the critical-layer interaction gradually evolves from a resonant triad of

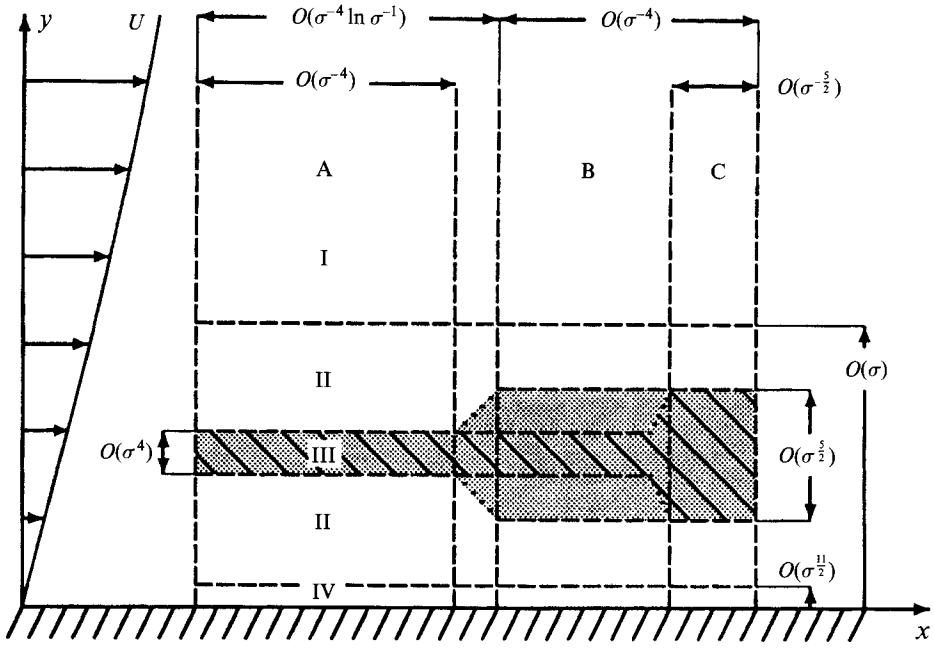

FIGURE 1. Asymptotic structure of the unsteady boundary-layer flow. I, main boundary layer; II, inviscid Tollmien wall layer; III, critical layers (hatched, fundamental; shaded, subharmonic); IV, (passive) Stokes layer. A, initial parametric-resonance stage; B, nonlinear-fundamental stage; C, fully coupled stage.

initially non-interacting instability waves on a decelerating boundary-layer flow. The triad consists of a two-dimensional fundamental mode and a pair of equal-amplitude oblique subharmonic modes, all of which are small-growth-rate solutions to the Rayleigh stability problem. The motion outside the critical layer remains a linear perturbation of the steady two-dimensional adverse-pressure-gradient boundary-layer flow. The wave-interaction effects are confined to a critical layer which evolves through a number of different stages (see figure 1). The initial parametric-resonance stage is analysed in §3. The two-dimensional fundamental mode continues to exhibit linear growth in this stage and the initial wave interaction is weak in the sense that it enters as an inhomogeneous term in an appropriate critical-layer problem rather than as a coefficient in the leading-order advection/diffusion operator. The subharmonic amplitude is explicitly determined by a single integro-differential equation which is solved analytically in Appendix B. The downstream asymptotic expansion of this solution determines the scaling for the next stage of evolution in which the fundamental becomes nonlinear. This occurs when the amplitude of the fundamental is $\propto$ (pressure gradient)$^{\frac{2}{3}}$. The subharmonic, whose growth is now controlled by parametric-resonance effects, evolves on a much shorter streamwise scale than the fundamental. Its critical layer is, therefore, much thicker than that of the fundamental.

The relevant critical-layer problems are formulated in §4, where it is shown that the fundamental is now governed by a viscous generalization of the strongly nonlinear inviscid non-equilibrium critical-layer problem derived in Goldstein, Durbin & Leib

(1987).† The subharmonic-amplitude equation can again be solved analytically. Its solution is given by the downstream asymptotic expansion of the solution for the previous stage – but with the linearly growing fundamental amplitude replaced by the corresponding strongly nonlinear critical-layer solution. This result shows that the subharmonic continues to grow even when the self-interaction effects drive the fundamental growth rate towards zero. It follows that the assumed asymptotic structure eventually must become invalid and, consequently, a new stage of development must occur. In this stage, the subharmonic reacts back on the fundamental and both waves evolve on the same shorter streamwise lengthscale. This means that the fundamental and subharmonic critical layers are again of equal thickness. This fully coupled stage is analysed in §5 where the relevant amplitude equations are shown to be the same as in G&L – but with the linear growth terms omitted. Finally, the results are discussed in §§6 and 7.

2. Formulation

2.1. *Problem statement*

The basic boundary-layer flow is taken to be two-dimensional and incompressible with free-stream velocity $U_e(s)$, where s measures the distance along the solid boundary from the leading edge (or stagnation point). The coordinates, time, all velocity components, and pressure are non-dimensionalized by ℓ, $\ell/U_e(L)$, $U_e(L)$, and $\rho_o U_e^2(L)$, respectively, where L is the downstream distance to a point in the region where the instability waves first interact,

$$\ell = \left(2\nu \int_0^L U_e \mathrm{d}s\right)^{\frac{1}{2}} / U_e(L) \tag{2.1}$$

is a lengthscale characteristic of the local boundary-layer thickness, and ρ_o and ν are the density and kinematic viscosity of the fluid. The origin of the non-dimensional coordinate system (x, y, z), which measures the distance in the streamwise, transverse and spanwise directions, is attached to the wall at $s = L$. Changes in the base flow then take place on the long viscous scale

$$x_3 = x/Re_\ell, \tag{2.2}$$

where $Re_\ell = \ell U_e(L)/\nu$ is a local Reynolds number based on ℓ, and are described by the laminar boundary-layer equations. The normalized base-flow pressure gradient $\mu = -U_e U_{e_{x_3}}$, where the subscript x_3 denotes differentiation with respect to that variable, is taken to be a small positive quantity. Curvature effects are assumed to be smaller still and will be neglected herein.

The local Reynolds number is assumed to be large enough so that the unsteady flow is nearly unaffected by the viscous boundary-layer growth over the entire streamwise region in which the nonlinear interaction takes place. Consequently, the streamwise base-flow velocity $U(x_3, y)$ can be treated as a function of the transverse coordinate y only, the transverse base-flow velocity $V(x_3, y)$ $[= O(Re_\ell^{-1})]$ does not enter into the unsteady problem, and the base-flow pressure $P(x_3) = \frac{1}{2}(1 - U_e^2)$ is essentially constant. Since μ is assumed to be small, U can be treated as a perturbation about

† See Maslowe (1986) for a review of nonlinear critical layers. Benney & Maslowe (1975) were the first to discuss growth-rate effects but they only did so in the context of an equilibrium critical layer.

the Blasius profile U_0, i.e.

$$U = U_0 - \sigma^2\bar{\mu}U_1 + \dots\,, \tag{2.3}$$

and the corresponding expression for the scaled wall-shear stress can be written as

$$\hat{\lambda}_w = \lambda_0 - \sigma^2\bar{\mu}\lambda_1 + \dots\,, \tag{2.4}$$

where $\lambda_0 = 0.46960$ is the Blasius value and $\sigma \ll 1$ is related to μ through $\mu = \sigma^2\bar{\mu}$ with $\bar{\mu} = O(1)$.

As in G&L, the upstream unsteady flow consists of an essentially inviscid resonant triad of non-interacting spatially growing instability waves – a single two-dimensional fundamental mode and two equal-amplitude subharmonic oblique modes that form a standing wave in the spanwise direction. Expanding (2.3) about $y = 0$ shows that the distance of the base-flow inflection point from the wall is $O(\sigma)$. This implies that the most unstable instability waves must have $O(\sigma^{-1})$ wavelengths and $O(\sigma^4)$ spatial growth rates (Reid 1965). Then, each of the three modes will have a distinct critical layer centred about the transverse position where the real part of its phase velocity equals the streamwise base-flow velocity. But since the resonance condition requires that the instability waves have nearly equal phase speeds, the critical levels coincide with the required degree of approximation. Putting

$$R = \sigma^{13}Re_\ell = O(1) \tag{2.5}$$

ensures that viscous effects will enter the critical-layer dynamics at the same order as the linear-growth effects, but will not affect the unsteady motion outside the critical layers (to the required order of approximation).

2.2. *The main boundary-layer region*

Since the unsteady flow remains essentially linear in the main part of the boundary layer, the total flow in this region is effectively

$$\begin{pmatrix} u \\ v \\ w \\ p \end{pmatrix} = \begin{pmatrix} U \\ 0 \\ 0 \\ 0 \end{pmatrix} + \mathrm{Re}\left[\mathscr{A}(x_2)\mathrm{e}^{\mathrm{i}X}\begin{pmatrix} \hat{u}_0 \\ \hat{v}_0 \\ 0 \\ \hat{p}_0 \end{pmatrix}\right]$$

$$+\mathrm{Re}\left[\mathscr{B}(x_2)\mathrm{e}^{\mathrm{i}X/2}\begin{pmatrix} \hat{u}_1\cos Z \\ \hat{v}_1\cos Z \\ \hat{w}_1\sin Z \\ \hat{p}_1\cos Z \end{pmatrix} + \begin{pmatrix} \mathscr{G} \\ 0 \\ 0 \\ 0 \end{pmatrix}\mathrm{e}^{\mathrm{i}2Z}\right] + \dots, \tag{2.6}$$

where $\boldsymbol{u} = (u, v, w)$ is the velocity, p is the pressure,

$$x_2 = \sigma^4 x \tag{2.7}$$

is the slow streamwise scale on which the linear growth occurs, $\mathscr{A}(x_2) \ll 1$ and $\mathscr{B}(x_2) \ll 1$ are slowly varying amplitude functions for the fundamental and the subharmonic, respectively, and $\mathscr{G}(x_2, y) \ll 1$ is a mean-flow correction that only enters in the fully coupled stage. Also,

$$X = \sigma\bar{\alpha}(x - \sigma\bar{c}t), \tag{2.8}$$

$$Z = \sigma\bar{\beta}(1 + \sigma^3\chi)z, \tag{2.9}$$

where $\bar{\alpha}$, $\bar{\beta}$ and $\bar{c}$ are the scaled streamwise and spanwise wavenumbers and phase speed correct up to but not including $O(\sigma^3)$ terms, and χ is a scaled (relative) spanwise

wavenumber detuning of the subharmonic disturbance. $\bar{S} = \bar{\alpha}\bar{c}$ is the scaled Strouhal number, or (non-dimensional) angular frequency, of the fundamental disturbance. $\hat{u}_n$, $\hat{v}_n$, $\hat{w}_n$, and $\hat{p}_n$ are functions of y that are determined by the usual inviscid three-dimensional instability equations to the required level of approximation. Hence,

$$\hat{u}_n = \frac{1}{\alpha_n k_n (U - c_n)} \left[\alpha_n^2 (U - c_n) \mathrm{D}\hat{\phi}_n + \beta_n^2 \mathrm{D}U \hat{\phi}_n\right], \tag{2.10}$$

$$\hat{v}_n = -\mathrm{i} k_n \hat{\phi}_n, \tag{2.11}$$

$$\hat{w}_n = \frac{-\mathrm{i}\beta_n}{\alpha_n (U - c_n)} \hat{p}_n, \tag{2.12}$$

$$\hat{p}_n = \frac{\alpha_n}{k_n} \left[\mathrm{D}U \hat{\phi}_n - (U - c_n)\mathrm{D}\hat{\phi}_n\right], \tag{2.13}$$

for $n = 0, 1$, where D denotes differentiation with respect to y. The $\hat{\phi}_n$ are governed by the Rayleigh equations

$$(U - c_n)(\mathrm{D}^2 - k_n^2)\hat{\phi}_n - \mathrm{D}^2 U \hat{\phi}_n = 0 \quad \text{for} \quad n = 0, 1, \tag{2.14}$$

subject to the boundary conditions $\hat{\phi}_n(0) = 0$ and $\hat{\phi}_n \to 0$ as $y \to +\infty$; $(1 + n)c_n = \sigma^2 \bar{S}/\alpha_n$,

$$\alpha_0 = \sigma \left[\bar{\alpha} - \sigma^3 \mathrm{i} (\ln \mathscr{A})'\right], \tag{2.15}$$

$$\alpha_1 = \sigma \left[\bar{k} \cos\theta - \sigma^3 \mathrm{i} (\ln \mathscr{B})'\right], \tag{2.16}$$

$k_n^2 = \alpha_n^2 + \beta_n^2$, $\beta_0 = 0$, $\beta_1 = \sigma\bar{\beta}(1 + \sigma^3\chi)$, $\bar{k}^2 = \frac{1}{4}\bar{\alpha}^2 + \bar{\beta}^2$, $\theta = \arctan(2\bar{\beta}/\bar{\alpha})$ and the prime denotes differentiation with respect to x_2. The resonance condition, $c_0 = c_1 + O(\sigma^4)$, for the upstream linear stage, implies that

$$\bar{k} = \bar{\alpha} \tag{2.17}$$

and, consequently, that $\theta = \frac{1}{3}\pi$.

The relevant asymptotic solution to (2.14) is most easily constructed by re-expanding the long-wavelength solution of Miles (1962) (see Reid 1965) for small c_n (Graebel 1966; Goldstein *et al.* 1987; G&L; and others). However, the result is not uniformly valid as $y \to 0$ and a separate solution to (2.14) must be constructed in a thin wall layer, which also contains the critical layer.

2.3. *The inviscid Tollmien wall layer*

To this end, the scaled transverse coordinate

$$Y = y/\sigma \tag{2.18}$$

is substituted into (2.14), using (2.15) and (2.16), to show that the solution in this region satisfying the inviscid boundary condition at $Y = 0$ is

$$\hat{\phi}_n = \sigma \left\{\lambda_0 Y + \sigma^r \left[a_n^{\pm}(Y - Y_c) + a_n^{-} Y_c\right] + \sigma^3 \left[F + b_n^{\pm}(Y - Y_c) + b_n^{-} Y_c\right]\right\}, \tag{2.19}$$

$$F = \bar{\mu}_c \left[\tfrac{1}{2} Y^2 + Y_c (Y - Y_c) \ln|Y - Y_c| + Y_c^2 \ln Y_c\right] - \tfrac{1}{24}\lambda_0^2 Y^3 (Y + 2Y_c), \tag{2.20}$$

where $0 < r < 3$, $\bar{\mu}_c = \bar{\mu} - \frac{1}{2}(\lambda_0 Y_c)^2$ is a scaled base-flow vorticity gradient at the critical level $y_c = \sigma Y_c$ and the $\pm$ superscript indicates different values for $Y \gtrless Y_c$. The discontinuity in the solution (2.19) results in a jump in the streamwise perturbation

velocity component,

$$\Delta\hat{u}_n = \frac{\alpha_n}{k_n}\left[\sigma^r(a_n^+ - a_n^-) + \sigma^3(b_n^+ - b_n^-)\right] = \frac{\mathrm{i}\alpha_n}{k_n^2}\Delta\left(\frac{\partial\hat{v}_n}{\partial y}\right), \tag{2.21}$$

across the critical layer. The integration constants $a_n^{\pm}$ and $b_n^{\pm}$ (which are at most functions of the long streamwise scale over which the wave growth occurs) and the exponent r are determined by matching this jump with the one induced by the critical layer. The velocity jump at $O(\sigma^r)$ is introduced to balance a wave-interaction-induced critical-layer velocity jump that occurs at a lower order than the $O(\sigma^3)$ jump associated with linear-growth effects. The $a_n^{\pm}$ can be set equal to zero in the initial parametric-resonance stage since the lower-order jump only occurs in the later stages of evolution.

2.4. *Matching*

Setting $a_n^{\pm} = 0$ and matching the main-boundary-layer and inviscid-Tollmien-wall-layer solutions to $O(\sigma^4 \ln\sigma)$ shows that

$$\bar{\alpha} = \bar{\alpha}_0 + \sigma\bar{\alpha}_1 + \sigma^2\bar{\alpha}_2 + \sigma^3 \ln\sigma\ \bar{\alpha}_{3L}, \tag{2.22}$$

where

$$\bar{\alpha}_0 = (\lambda_0\bar{S})^{\frac{1}{2}}, \tag{2.23}$$

$$\bar{\alpha}_1 = (1 - \tfrac{1}{2}J_1)\bar{S}, \tag{2.24}$$

$$\bar{\alpha}_2 = -\tfrac{1}{2}\left(\bar{S}/\lambda_0\right)^{\frac{1}{2}}\left\{\left[3J_1\left(1 - \tfrac{5}{12}J_1\right) + 2J_2 + J_3\right]\bar{S} + \bar{\mu}\lambda_1\right\}, \tag{2.25}$$

$$\bar{\alpha}_{3L} = \left(\bar{\mu} - \bar{S}/2\lambda_0\right)\bar{S}/2\lambda_0^2, \tag{2.26}$$

and J_1, J_2, and J_3 are certain integrals that only depend on the Blasius profile and are given in Goldstein (1983, p. 71). They take on the numerical values 0.928 09, −2.093 22, and 1.287 77, respectively. Matching the solution to $O(\sigma^5)$ shows that the scaled velocity jump for the fundamental is

$$b_0^+ - b_0^- = \Lambda M_0\left[\kappa_i + \mathrm{i}\,(\ln\mathscr{A})'\right], \tag{2.27}$$

where $\Lambda = 2\lambda_0^2\bar{S}/\bar{\alpha}^3$,

$$M_0 = 1 + \sigma\left(3 - \tfrac{1}{2}J_1\right)\left(\bar{S}/\lambda_0\right)^{\frac{1}{2}} + O(\sigma^2), \tag{2.28}$$

and κ_i is a real constant that is fully determined by the matching but its explicit form is not given here because it is not used in the subsequent analysis.

2.5. *The Stokes layer*

As usual, a completely passive Stokes layer is induced by the no-slip boundary condition at the wall. The relevant solution in this region is

$$\hat{\phi}_n = \sigma\lambda_0\left[Y + \sigma^{\frac{9}{2}}\mathrm{e}^{\mathrm{i}\frac{\pi}{4}}\left(\frac{n+1}{R\bar{S}}\right)^{\frac{1}{2}}\left\{\exp\left[-\mathrm{e}^{-\mathrm{i}\frac{\pi}{4}}\left(\frac{R\bar{S}}{n+1}\right)^{\frac{1}{2}}\frac{Y}{\sigma^{\frac{9}{2}}}\right] - 1\right\}\right], \tag{2.29}$$

which shows that the Stokes-layer thickness is $O(\sigma^{\frac{11}{2}})$ relative to the width of the boundary layer.

2.6. *The critical layer*

As already indicated, the wave-interaction effects are confined to the critical layer and, at least for the subharmonic, are weak in the sense that they enter through inhomogeneous terms in an appropriate critical-layer problem rather than though a coefficient in the leading-order advection/diffusion operator. This ultimately implies that the subharmonic amplitude $\mathscr{B}$ can be determined from equations involving only a single independent variable, which in the present case turn out to be of the integro-differential type. As in studies of more conventional weakly nonlinear flows (Benney & Gustavsson 1981; and others), these equations are most easily derived by first rewriting the governing equations, i.e. the equation of continuity and the (viscous) momentum equation, in a somewhat different form. This amounts to taking the divergence of the momentum equation to obtain an equation for the Laplacian of the pressure, then combining the transverse derivative of this equation with the Laplacian of the transverse component of the momentum equation to eliminate the pressure terms and thereby obtain

$$\left(\frac{\partial}{\partial t}+\boldsymbol{u}\cdot\nabla-\frac{1}{Re_\ell}\nabla^2\right)\nabla^2 v-\nabla^2\boldsymbol{u}\cdot\nabla v=2\left[\frac{\partial}{\partial x}J(v,w)-\frac{\partial}{\partial y}J(u,w)+\frac{\partial}{\partial z}J(u,v)\right], \quad (2.30)$$

where ∇^2 is the Laplacian and $J(\cdot,\cdot)\equiv\partial(\cdot,\cdot)/\partial(x,z)$ is a horizontal Jacobian derivative. Since $\nabla^2 v$ is the transverse component of the curl of the (total) vorticity $\nabla\times\boldsymbol{u}$, (2.30) describes the dynamics of the horizontal vorticity components. This approach is related to the one used by Wu (1992) in that the transverse velocity component is the 'primary' dependent variable in the critical layer.

3. Initial parametric-resonance stage

The streamwise region of primary interest is the one in which the fundamental is strongly nonlinear. Since the solution in this region does not involve a subharmonic that can be matched onto a corresponding wave in the upstream linear region (in which all the waves are decoupled), it is necessary to introduce an intermediate parametric-resonance stage. The fundamental is completely linear in this stage and both waves evolve on the long scale x_2. Then, as shown in G&L, linear-growth and parametric-resonance effects will enter the critical-layer dynamics at the same order if

$$\mathscr{A}=\sigma^{13}\bar{A},(x_2)\qquad \bar{A}=O(1). \quad (3.1)$$

The subharmonic scaling,

$$\mathscr{B}=\delta\bar{B},(x_2)\qquad \bar{B}=O(1), \quad (3.2)$$

is worked out in §5. For now, it is sufficient to note that δ is small enough to avoid back-reaction of the subharmonic on the fundamental.

As indicated above, the $a_n^{\pm}$ can be set equal to zero in the Tollmien solutions (2.19) and (2.20) in the present region. Matching with the main boundary-layer flow then shows that the subharmonic velocity jump is given by

$$b_1^+-b_1^-=A\left\{M_0\left[\kappa_i-\tfrac{3}{8}\chi(\lambda_0\bar{S})^{\frac{1}{2}}\right]+\tfrac{5}{4}\mathrm{i}M_1\left(\ln\bar{B}\right)'\right\}, \quad (3.3)$$

where

$$M_1=1+\sigma^{\frac{4}{5}}\left(\tfrac{9}{2}-J_1\right)\left(\bar{S}/\lambda_0\right)^{\frac{1}{2}}+O(\sigma^2). \quad (3.4)$$

Linear-growth effects can only influence the critical-layer dynamics when the thickness of this layer is of the same order as the linear growth rate, i.e. $O(\sigma^4)$. The appropriate transverse coordinate for this region is therefore

$$\eta = (y - y_c)/\sigma^4 = (Y - Y_c)/\sigma^3. \tag{3.5}$$

The limits as $Y \to Y_c\pm$ of the Tollmien solutions, (2.19) and (2.20), show that the critical-layer flow expands like

$$u = \sigma\left[\bar{c} + \sigma^3\lambda_w\eta + \sigma^6\bar{\mu}_c^\dagger Y_c\eta + \sigma^9\left(\tfrac{1}{2}\bar{\mu}_c\eta^2 - \bar{c}x_2R^{-1}\right)\right] + \sigma^{13}\mathrm{Re}\left[\left(\hat{\bar{u}}_0^{(1)} + \sigma^3\hat{\bar{u}}_0^{(2)}\right)\bar{A}\mathrm{e}^{\mathrm{i}X}\right] + \delta\sigma^{-3}\bar{u}_1^{(0)}\cos Z + \dots, \tag{3.6}$$

$$v = \sigma^{15}\tfrac{1}{2}\lambda_0 Y_c^2 R^{-1} + \sigma^{15}\mathrm{Re}\left[\left(-\mathrm{i}\bar{\alpha}\lambda_0 Y_c + \sigma^3\hat{\bar{v}}_0^{(1)}\right)\bar{A}\mathrm{e}^{\mathrm{i}X}\right] + \delta\sigma^2\left\{\mathrm{Re}\left[\left(-\mathrm{i}\bar{k}\lambda_0 Y_c + \sigma^3\hat{\bar{v}}_1^{(1)}\right)\bar{B}\mathrm{e}^{\mathrm{i}X/2}\right] + \sigma^6\bar{v}_1^{(2)}\right\}\cos Z + \dots, \tag{3.7}$$

$$p = \sigma^{11}\bar{\mu}x_2R^{-1} + \sigma^{14}\mathrm{Re}\left(\lambda_0\bar{c}\bar{A}\mathrm{e}^{\mathrm{i}X}\right) + \delta\sigma\mathrm{Re}\left(\tfrac{1}{2}\lambda_0\bar{c}\bar{B}\mathrm{e}^{\mathrm{i}X/2}\right)\cos Z + \dots, \tag{3.8}$$

where the ellipsis denote higher-order terms for the basic, fundamental, and subharmonic components of the flow and $\bar{\mu}_c^\dagger = \bar{\mu} - \frac{1}{6}(\lambda_0 Y_c)^2$. The expansion for the spanwise velocity w is analogous to the subharmonic part of (3.6) and, therefore, is not written out explicitly. $\hat{\bar{u}}_0^{(1)}$, $\hat{\bar{v}}_0^{(1)}$, and $\hat{\bar{v}}_1^{(1)}$ possess expansions in terms of σ, containing terms up to and including $O(\sigma^3\ln\sigma)$. They are given by the relevant terms in the inner limit of the Tollmien solutions. $\hat{\bar{u}}_0^{(1)}$ is independent of η, whereas $\hat{\bar{v}}_0^{(1)}$ and $\hat{\bar{v}}_1^{(1)}$ are linear functions of η. The non-parallel base-flow terms in (3.6) and (3.7) and the streamwise pressure-gradient term in (3.8) do not affect the critical-layer dynamics.

Substitution of the expansions (3.6) and (3.7) into the spanwise vorticity equation produces, for the fundamental,

$$\bar{\mathscr{L}}_2\left(\frac{\partial\hat{\bar{u}}_0^{(2)}}{\partial\eta}\bar{A}\mathrm{e}^{\mathrm{i}X}\right) = \mathrm{i}\bar{\mu}_c\bar{S}\bar{A}\mathrm{e}^{\mathrm{i}X}, \tag{3.9}$$

where

$$\bar{\mathscr{L}}_2 = \bar{c}\frac{\partial}{\partial x_2} + \bar{\alpha}\lambda_0\eta\frac{\partial}{\partial X} - \frac{1}{R}\frac{\partial^2}{\partial\eta^2} \tag{3.10}$$

is the leading-order advection/diffusion operator in the critical layer; and substitution of the expansions (3.6)–(3.8) into the streamwise momentum equation and (2.30) produces, for the subharmonic,

$$\bar{\mathscr{L}}_2\bar{u}_1^{(0)} = \tfrac{3}{4}\lambda_0\bar{S}\mathrm{Re}\left(\mathrm{i}\bar{B}\mathrm{e}^{\mathrm{i}X/2}\right), \tag{3.11}$$

$$\bar{\mathscr{L}}_2\frac{\partial^2\bar{v}_1^{(2)}}{\partial\eta^2} = \tfrac{1}{2}\bar{\mu}_c\bar{\alpha}\bar{S}\mathrm{Re}\left(\bar{B}\mathrm{e}^{\mathrm{i}X/2}\right) + \bar{\alpha}\bar{S}\mathrm{Re}\left(\bar{A}\mathrm{e}^{\mathrm{i}X}\right)\frac{\partial^2\bar{u}_1^{(0)}}{\partial\eta^2}. \tag{3.12}$$

Integration of $\bar{A}\mathrm{e}^{\mathrm{i}X}\partial\hat{\bar{u}}_0^{(2)}/\partial\eta$ and $\partial^2\bar{v}_1^{(2)}/\partial\eta^2$ across the critical layer and using (2.21) produces the following expressions for the scaled velocity jumps $b_0^+ - b_0^-$ and $b_1^+ - b_1^-$:

$$\int_{-\infty}^{+\infty}\frac{\partial\hat{\bar{u}}_0^{(2)}}{\partial\eta}\mathrm{d}\eta = b_0^+ - b_0^-, \tag{3.13}$$

$$\frac{1}{2\pi}\int_{-\infty}^{+\infty}\int_0^{4\pi}\frac{\partial^2\bar{v}_1^{(2)}}{\partial\eta^2}\mathrm{e}^{-\mathrm{i}X/2}\mathrm{d}X\mathrm{d}\eta = -\mathrm{i}\bar{k}\left(b_1^+ - b_1^-\right)\bar{B}. \tag{3.14}$$

Combining these expressions with those obtained from the flow outside the critical layer, i.e. (2.27) and (3.3), then gives the matching conditions

$$\bar{A}\int_{-\infty}^{+\infty}\frac{\partial\hat{\bar{u}}_0^{(2)}}{\partial\eta}\mathrm{d}\eta = \Lambda M_0\left(\kappa_i\bar{A}+\mathrm{i}\bar{A}'\right), \tag{3.15}$$

$$\frac{1}{2\pi}\int_{-\infty}^{+\infty}\int_0^{4\pi}\frac{\partial^2\bar{v}_1^{(2)}}{\partial\eta^2}\mathrm{e}^{-\mathrm{i}X/2}\mathrm{d}X\mathrm{d}\eta = \bar{\alpha}\Lambda\left\{\tfrac{5}{4}M_1\bar{B}'-\mathrm{i}M_0\left[\kappa_i-\tfrac{3}{8}\chi(\lambda_0\bar{S})^{\frac{1}{2}}\right]\bar{B}\right\}. \tag{3.16}$$

Equations (3.9) and (3.15) correspond to the linear-growth critical layer and therefore possess the simple solution

$$\bar{A} = \bar{A}_0\mathrm{e}^{\kappa x_2}, \tag{3.17}$$

where $\bar{A}_0$ is a constant and $\kappa = \kappa_r + \mathrm{i}\kappa_i$, with

$$\kappa_r = \pi\bar{\alpha}^2\bar{\mu}_c/2\lambda_0^3 M_0 \tag{3.18}$$

being the linear growth rate.

Equations (3.11) and (3.12) are solved in Appendix A. Substitution of the result into the velocity-jump condition (3.16) leads to

$$\bar{B}' = \tfrac{4}{5}\varkappa\left[\kappa-\tfrac{3}{8}\mathrm{i}\chi(\lambda_0\bar{S})^{\frac{1}{2}}\right]\bar{B} + 4\mathrm{i}\gamma\kappa_r^4\int_{-\infty}^{x_2}(x_2-\xi)^2\mathrm{e}^{-\kappa_r^3(x_2-\xi)^3/6\bar{R}}\bar{A}(\xi)\bar{B}^*(2\xi-x_2)\mathrm{d}\xi, \tag{3.19}$$

where the asterisk denotes complex conjugation, $\varkappa = M_0/M_1$,

$$\gamma = 3\pi\bar{\alpha}^7/80\bar{S}^2\kappa_r^4 M_1, \tag{3.20}$$

and

$$\bar{R} = \bar{S}^3\kappa_r^3 R/\lambda_0^2\bar{\alpha}^5 \tag{3.21}$$

is a rescaled critical-layer Reynolds number. Equation (3.19) implies that

$$\bar{B}\to\bar{B}_0\exp\left\{\tfrac{4}{5}\varkappa\left[\kappa-\tfrac{3}{8}\mathrm{i}\chi(\lambda_0\bar{S})^{\frac{1}{2}}\right]x_2\right\}\quad\text{as}\quad x_2\to-\infty, \tag{3.22}$$

where $\bar{B}_0$ is a constant. This shows that $\bar{B}$ matches onto the appropriate linear-growth critical-layer solution.

An analytic solution to (3.19) is derived in Appendix B. Its large-x_2 asymptotic expansion is given by (B 20), which can be renormalized to obtain

$$\bar{B}\to\frac{\bar{B}_\infty^\dagger|\bar{B}_0|}{(\gamma|\bar{A}_0|)^{\frac{1}{5}\varkappa}}\exp\left[\tfrac{1}{5}\varkappa\kappa_r x_2+\kappa_r\int_{-\infty}^{x_2}(\gamma|\bar{A}|)^{\frac{1}{5}}\mathrm{d}\xi+\tfrac{1}{2}\mathrm{i}\arg(\mathrm{i}\bar{A})\right]\quad\text{as}\quad x_2\to+\infty. \tag{3.23}$$

Equations (3.17) and (3.23) show that the subharmonic growth rate becomes exponentially large as $x_2\to+\infty$.

4. Nonlinear-fundamental stage

Since (3.17) and (3.23) imply that the fundamental and subharmonic continue to grow with increasing x_2, the solutions of the preceding section must eventually become invalid. In the present analysis, this occurs when the nonlinear convection of vorticity becomes of the same order as the linear-growth effects within the critical layer for the fundamental, i.e. as shown by Goldstein *et al.* (1987), when $\mathscr{A} = O(\sigma^7)$

or equivalently when $x_2 = O(\ln \sigma^{-6})$. Equations (3.17) and (3.23) suggest that the fundamental and subharmonic amplitude functions should then be of the form

$$\mathscr{A} = \sigma^7 A(x_2^+)\mathrm{e}^{-\mathrm{i}X_0}, \qquad A = O(1), \tag{4.1}$$

$$\mathscr{B} = \delta\sigma^{-\frac{6}{5}} B \exp\left[\sigma^{-\frac{3}{2}}\Phi(x_2^+) - \tfrac{1}{2}\mathrm{i}X_0\right], \qquad B = O(1), \qquad \Phi = O(1), \tag{4.2}$$

where

$$B = B^{(0)}(x_2^+) + \sigma^{\frac{3}{2}} B^{(1)}(x_2^+) + \ldots, \tag{4.3}$$

$$x_2^+ = x_2 + 6\kappa_r^{-1}\ln\sigma, \qquad x_2^+ = O(1), \tag{4.4}$$

$X_0 = 6\kappa_i\kappa_r^{-1}\ln\sigma$ is minus the fundamental phase shift over the initial-parametric-resonance region, and Φ turns out to be purely real. $\mathscr{A}$ can be of the usual multiple-scales form, but $\mathscr{B}$ must be allowed to take on a more general WKBJ form in order to deal with the shorter (but still much longer than a wavelength) spatial scale induced by its asymptotically larger growth rate *vis-à-vis* that of the fundamental. The subharmonic amplitude $\mathscr{B}$ is required to be $o(\sigma^{\frac{11}{2}})$ throughout the present streamwise region in order to preclude back-reaction of the subharmonic on the fundamental.

The inviscid Tollmien solution for the fundamental is still given by (2.19)–(2.22) with $a_0^{\pm} = 0$, since its critical-layer velocity jump (which is now induced by the self-interaction effects) is $O(\sigma^3)$. However, the appropriate inviscid Tollmien solution for the subharmonic is given by (2.19)–(2.22) with $r = \frac{3}{2}$ and $a_1^{\pm} \neq 0$, since the velocity jump induced by the parametric-resonance effects is now $O(\sigma^{\frac{3}{2}})$. Matching with the main boundary-layer region shows that the subharmonic velocity jumps are now given by

$$a_1^+ - a_1^- = \tfrac{5}{4}\mathrm{i}AM_1\Phi', \tag{4.5}$$

$$b_1^+ - b_1^- = 2\left(\lambda_0/\bar{S}\right)^{\frac{1}{2}}\left[\kappa_i + \tfrac{5}{4}\mathrm{i}\,(\ln B)'\right] - \tfrac{3}{4}\lambda_0\chi + \tfrac{5}{2}\mathrm{i}a_1^-\left(\lambda_0\bar{S}\right)^{-\frac{1}{2}}\Phi' - \tfrac{79}{8}\bar{S}^{-1}\Phi'^2. \tag{4.6}$$

Since the thickness of the fundamental critical layer remains $O(\sigma^4)$, even though the vorticity balance differs from the preceding stage, its relevant scaled transverse coordinate is still given by (3.5). The subharmonic critical-layer thickness, which is determined by the balance of growth and base-flow convection effects, is now $O(\sigma^{\frac{5}{2}})$, since the subharmonic growth rate $\mathscr{B}^{-1}\mathrm{d}\mathscr{B}/\mathrm{d}x = \sigma^{\frac{5}{2}}\Phi' + \ldots$. The appropriate scaled transverse coordinate for this 'outer' critical layer is therefore

$$\tilde{\eta} = (y - y_c)/\sigma^{\frac{5}{2}} = (Y - Y_c)/\sigma^{\frac{3}{2}}, \tag{4.7}$$

which reflects the fact that the fundamental and the subharmonic critical levels coincide. The fundamental remains linear in this outer critical layer and is therefore given by the inner limit of the corresponding inviscid Tollmien solution for $\tilde{\eta} = O(1)$.

4.1. *The critical layer for the fundamental*

The inner-critical-layer expansions are essentially a reordering of the linear-critical-layer expansions of the preceding section. They are now

$$u = \sigma\left[\bar{c} + \sigma^3\lambda_w\eta + \sigma^6\bar{\mu}_c^{\dagger}Y_c\eta + \sigma^9\left(\tfrac{1}{2}\bar{\mu}_c\eta^2 - \bar{c}x_2R^{-1}\right)\right] + \sigma^7\left[\mathrm{Re}\left(\hat{\bar{u}}_0^{(1)}A\mathrm{e}^{\mathrm{i}X^+}\right) + \sigma^3 u_0^{(2)}\right] + \ldots + \text{s.t.}, \tag{4.8}$$

$$v = \sigma^{15}\tfrac{1}{2}\lambda_0 Y_c^2 R^{-1} + \sigma^9\mathrm{Re}\left[\left(-\mathrm{i}\bar{\alpha}\lambda_0 Y_c + \sigma^3\hat{\bar{v}}_0^{(1)}\right)A\mathrm{e}^{\mathrm{i}X^+}\right] + \ldots + \text{s.t.}, \tag{4.9}$$

$$p = \sigma^{11}\bar{\mu}x_2R^{-1} + \sigma^8\mathrm{Re}\left(\lambda_0\bar{c}A\mathrm{e}^{\mathrm{i}X^+}\right) + \ldots + \text{s.t.}, \tag{4.10}$$

where $X^+ = X - X_0$, $\hat{\tilde{u}}_0^{(1)}$ and $\hat{\tilde{v}}_0^{(1)}$ are the same as in the preceding section, and s.t. indicates terms associated with the subharmonic disturbance which do not influence the dynamics of the fundamental in this streamwise region. As before, the base-flow-divergence and pressure-gradient terms are purely passive in these expansions.

Substitution of the expansions (4.8) and (4.9) into the spanwise vorticity equation yields

$$\mathscr{L}_2 \frac{\partial u_0^{(2)}}{\partial \eta} = \bar{\mu}_c \bar{S} \mathrm{Re}\left(\mathrm{i} A \mathrm{e}^{\mathrm{i}X^+}\right), \tag{4.11}$$

where

$$\mathscr{L}_2 = \bar{c}\frac{\partial}{\partial x_2^+} + \bar{\alpha}\lambda_0 \eta \frac{\partial}{\partial X^+} - \mathrm{Re}\left(\mathrm{i}\bar{S} A \mathrm{e}^{\mathrm{i}X^+}\right)\frac{\partial}{\partial \eta} - \frac{1}{R}\frac{\partial^2}{\partial \eta^2} \tag{4.12}$$

is the leading-order advection/diffusion operator in the inner critical layer. The difference from the linear problem (3.9) is due to the advection of unsteady spanwise vorticity by the transverse velocity component that now enters the vorticity balance.

Integrating $\partial u_0^{(2)}/\partial \eta$ across the critical layer and using (2.21) produces an expression for the velocity jump $b_0^+ - b_0^-$ in terms of the critical-layer solution, which is analogous to that given by (3.13). Combining this result with (2.27) yields the matching condition

$$\frac{1}{\pi}\int_{-\infty}^{+\infty}\int_0^{2\pi} \frac{\partial u_0^{(2)}}{\partial \eta} \mathrm{e}^{-\mathrm{i}X^+} \mathrm{d}X^+ \mathrm{d}\eta = \Lambda M_0 \left(\kappa_i A + \mathrm{i}A'\right). \tag{4.13}$$

Equations (4.11)–(4.13) are the viscous counterparts of the inviscid nonlinear 'unsteady' critical-layer equations derived in Goldstein *et al.* (1987). These equations are to be solved subject to the initial condition

$$A \to \bar{A}_0 \mathrm{e}^{\kappa x_2^+} \quad \text{as} \quad x_2^+ \to -\infty, \tag{4.14}$$

which ensures that the solution matches onto the upstream linear instability wave.

4.2. *The critical layer for the subharmonic*

The inner limits of the Tollmien-region solutions (2.19) and (2.20) show that the flow in the outer critical layer expands like

$$u = \sigma\left(\bar{c} + \sigma^{\frac{1}{2}}\lambda_w \tilde{\eta} + \sigma^{\frac{9}{2}}\bar{\mu}_c^{\dagger} Y_c \tilde{\eta} + \sigma^6 \tfrac{1}{2}\bar{\mu}_c \tilde{\eta}^2\right) + \sigma^7 \mathrm{Re}\left(\hat{u}_0^{(1)} A \mathrm{e}^{\mathrm{i}X^+}\right) + \tilde{\delta}\sigma^{-\frac{1}{2}}\left(u_1^{(0)} + \sigma^{\frac{1}{2}} u_1^{(1)}\right)\cos Z + \dots, \tag{4.15}$$

$$v = \sigma^{15}\tfrac{1}{2}\lambda_0 Y_c^2 R^{-1} + \sigma^9 \mathrm{Re}\left[-\mathrm{i}\bar{\alpha}\lambda_0\left(Y_c + \sigma^{\frac{1}{2}}\tilde{\eta}\right) A \mathrm{e}^{\mathrm{i}X^+}\right] + \tilde{\delta}\sigma^2\left\{\mathrm{Re}\left[\left(-\mathrm{i}\bar{k}\lambda_0 Y_c + \sigma^{\frac{1}{2}}\hat{v}_1^{(1)}\right) B E_+\right] + \sigma^3 v_1^{(2)} + \sigma^{\frac{9}{2}} v_1^{(3)}\right\}\cos Z + \dots, \tag{4.16}$$

$$w = \tilde{\delta}\sigma^{-\frac{1}{2}} w_1^{(0)} \sin Z + \dots, \tag{4.17}$$

$$p = \sigma^{11}\bar{\mu} x_2 R^{-1} + \sigma^8 \mathrm{Re}\left(\lambda_0 \bar{c} A \mathrm{e}^{\mathrm{i}X^+}\right) + \tilde{\delta}\sigma \mathrm{Re}\left[\left(\lambda_0 \bar{c} + \sigma^{\frac{1}{2}}\hat{p}_1^{(1)}\right) B E_+\right]\cos Z + \dots, \tag{4.18}$$

where $\tilde{\delta} = \delta/\sigma^{\frac{6}{5}}$ and $E_+ = \exp(\sigma^{-\frac{1}{2}}\Phi + \mathrm{i}X^+/2)$ have been introduced for clarity. $\hat{u}_0^{(1)}$, $\hat{v}_1^{(1)}$, and $\hat{p}_1^{(1)}$ possess expansions in terms of σ that are given by the corresponding terms in the inner limit of the Tollmien-region solutions. They are all constants, except $\hat{v}_1^{(1)}$ which is a linear function of $\tilde{\eta}$. The base-flow-divergence and pressure-gradient terms in (4.16) and (4.18) have no effect on the critical-layer dynamics.

Substitution of the expansions (4.3) and (4.15)–(4.18) into the continuity and streamwise momentum equations as well as (2.30) yields at 'leading-order'

$$w_1^{(0)} = -\frac{2}{\sqrt{3}}\frac{\partial u_1^{(0)}}{\partial X^+}, \tag{4.19}$$

$$\mathscr{L}_1 u_1^{(0)} = \tfrac{3}{4}\lambda_0 \bar{S}\mathrm{Re}\left(\mathrm{i}B^{(0)}E_+\right), \tag{4.20}$$

$$\mathscr{L}_1 \frac{\partial^2 v_1^{(2)}}{\partial \tilde{\eta}^2} = \bar{\alpha}\bar{S}\mathrm{Re}\left(A\mathrm{e}^{\mathrm{i}X^+}\right)\frac{\partial^2 u_1^{(0)}}{\partial \tilde{\eta}^2}, \tag{4.21}$$

where

$$\mathscr{L}_1 = \bar{c}\Phi' + \bar{\alpha}\lambda_0\tilde{\eta}\frac{\partial}{\partial X^+} \tag{4.22}$$

is the 'leading-order' approximation to the advection/diffusion operator in the outer critical layer. At 'next-order',

$$\mathscr{L}_1 u_1^{(1)} = \mathrm{Re}\left[\left(\tfrac{3}{4}\mathrm{i}\lambda_0\bar{S}B^{(1)} - \hat{q}_1^{(1)}B^{(0)}\right)E_+\right] - \mathscr{L}_1^{(1)}u_1^{(0)}, \tag{4.23}$$

$$\begin{aligned}\mathscr{L}_1\frac{\partial^2 v_1^{(3)}}{\partial\tilde{\eta}^2} = {} & \tfrac{1}{2}\bar{\mu}_c\bar{\alpha}\bar{S}\mathrm{Re}\left(B^{(0)}E_+\right) + \bar{\alpha}\mathrm{Re}\left(A\mathrm{e}^{\mathrm{i}X^+}\right)\left(\bar{S}\frac{\partial^2 u_1^{(1)}}{\partial\tilde{\eta}^2} + \bar{\alpha}\lambda_0\tilde{\eta}\frac{\partial^2 u_1^{(0)}}{\partial\tilde{\eta}^2}\right)\\ & - \mathscr{L}_1^{(1)}\frac{\partial^2 v_1^{(2)}}{\partial\tilde{\eta}^2} - 2\bar{\alpha}\bar{\beta}\lambda_0\mathrm{Re}\left(\mathrm{i}A\mathrm{e}^{\mathrm{i}X^+}\right)\frac{\partial w_1^{(0)}}{\partial\tilde{\eta}},\end{aligned} \tag{4.24}$$

where

$$\mathscr{L}_1^{(1)} = \bar{c}\frac{\partial}{\partial x_2^+} + \lambda_0\tilde{\eta}\Phi' \tag{4.25}$$

is the 'next-order' correction to the advection/diffusion operator and

$$\hat{q}_1^{(1)} = \lambda_0\hat{v}_1^{(1)} + \tfrac{1}{2}\mathrm{i}\bar{\alpha}\hat{p}_1^{(1)} + \tfrac{1}{2}\lambda_0\bar{c}\Phi' = -\tfrac{1}{8}\mathrm{i}\lambda_0\left(6\bar{\alpha}a_1^- Y_c - \mathrm{i}\bar{c}\Phi' + 8\bar{\alpha}\lambda_0\tilde{\eta}\right). \tag{4.26}$$

Using (2.21), after integrating $\partial^2 v_1^{(2)}/\partial\tilde{\eta}^2$ and $\partial^2\bar{v}_1^{(3)}/\partial\tilde{\eta}^2$ across the outer critical layer, produces the matching conditions

$$\frac{1}{2\pi}\int_{-\infty}^{+\infty}\int_0^{4\pi}\frac{\partial^2 v_1^{(2)}}{\partial\tilde{\eta}^2}E_+^{-1}\mathrm{d}X^+\mathrm{d}\tilde{\eta} = -\mathrm{i}\bar{\alpha}\left(a_1^+ - a_1^-\right)B^{(0)}, \tag{4.27}$$

$$\begin{aligned}\frac{1}{2\pi}\int_{-\infty}^{+\infty}\int_0^{4\pi}\frac{\partial^2 v_1^{(3)}}{\partial\tilde{\eta}^2}E_+^{-1}\mathrm{d}X^+\mathrm{d}\tilde{\eta} = {} & -\mathrm{i}\bar{\alpha}\left(a_1^+ - a_1^-\right)B^{(1)}\\ & - \left[\mathrm{i}\bar{\alpha}\left(b_1^+ - b_1^-\right) + \tfrac{1}{2}\left(a_1^+ - a_1^-\right)\Phi'\right]B^{(0)}.\end{aligned} \tag{4.28}$$

The 'leading-order' problem – as defined by (4.20), (4.21), and (4.27) – actually involves two levels of approximation since substitution of the expansion (2.22) (and the corresponding expansion for $\bar{c}$) into those equations produces an intermediate problem of lower order than the 'next-order' problem defined by (4.19), (4.23), and (4.24). However, it is easier to retain the higher-order terms and simply discard them at the end of the analysis by expanding the solution *a posteriori*.

4.3. *Solution of the 'leading-order' problem for the subharmonic*

Equations (4.20) and (4.21) imply that

$$u_1^{(0)} = \mathrm{Re}\left(\hat{u}_1^{(0)} E_+\right), \tag{4.29}$$

$$v_1^{(2)} = \mathrm{Re}\left[\left(\hat{v}_{1,1}^{(2)} + \hat{v}_{1,3}^{(2)} \mathrm{e}^{\mathrm{i}X^+}\right) E_+\right], \tag{4.30}$$

where $\hat{u}_1^{(0)}$, $\hat{v}_{1,1}^{(2)}$, and $\hat{v}_{1,1}^{(2)}$ depend on x_2 and $\tilde{\eta}$, and only the $\hat{v}_{1,1}^{(2)}$ term contributes to the velocity jump condition (4.27). Substituting (4.29) and (4.30) into (4.20) and (4.21), solving the resulting set of (relatively trivial) algebraic equations in sequence for $\hat{u}_1^{(0)}$ and $\hat{v}_{1,1}^{(2)}$, using the latter result to evaluate the integral in (4.27), and combining that result with (4.5) yields

$$\Phi'^4 B^{(0)} = \mathrm{i}\gamma\kappa_r^4 A B^{(0)*}. \tag{4.31}$$

Since Φ is real, this implies that

$$\Phi = \kappa_r \int_{-\infty}^{x_2^+} (\gamma|A|)^{\frac{1}{4}}\, \mathrm{d}\xi, \tag{4.32}$$

$$\arg B^{(0)} = \tfrac{1}{2}\arg(\mathrm{i}A), \tag{4.33}$$

which show that Φ matches the dominant exponential term in (3.23).

4.4. *Solution of the 'next-order' problem for the subharmonic*

Equations (4.19)–(4.24) imply that

$$w_1^{(0)} = \mathrm{Re}\left(\hat{w}_1^{(0)} E_+\right), \tag{4.34}$$

$$u_1^{(1)} = \mathrm{Re}\left(\hat{u}_1^{(1)} E_+\right), \tag{4.35}$$

$$v_1^{(3)} = \mathrm{Re}\left[\left(\hat{v}_{1,1}^{(3)} + \hat{v}_{1,3}^{(3)} \mathrm{e}^{\mathrm{i}X^+}\right) E_+\right], \tag{4.36}$$

where $\hat{w}_1^{(0)}$, $\hat{u}_1^{(1)}$, $\hat{v}_{1,1}^{(3)}$, and $\hat{v}_{1,1}^{(3)}$ depend on x_2 and $\tilde{\eta}$, and, again, only the $\hat{v}_{1,1}^{(3)}$ term of (4.36) contributes to the velocity jump (4.28). Substitution of (4.34)–(4.36) into (4.19)–(4.24) again leads to a set of algebraic equations which can be solved in sequence for $\hat{w}_1^{(0)}$, $\hat{u}_1^{(1)}$, and $\hat{v}_{1,1}^{(3)}$. The latter result can then be used to evaluate the integral in (4.28). This result, when combined with (4.5) and (4.6), yields

$$B^{(1)} = \mathrm{i}A|A|^{-1} B^{(1)*} + K, \tag{4.37}$$

where

$$K = -\Phi'^{-1}\left\{4B^{(0)'} - \tfrac{4}{5}\left[\kappa - \tfrac{3}{8}\mathrm{i}(\lambda_0\bar{S})^{\frac{1}{2}}\chi\right] B^{(0)} - \tfrac{3}{2}\mathrm{i}\,(\arg A)'\, B^{(0)}\right\}$$
$$- (\lambda_0\bar{c})^{-1}\left[\bar{c}\left(a_1^- - a_1^{-*}\right) + \tfrac{119}{20}\mathrm{i}\Phi'\right] B^{(0)}. \tag{4.38}$$

Taking the complex conjugate of (4.37) and substituting the resulting expression for $B^{(1)*}$ back into (4.37) leads to the following solvability condition:

$$K + \mathrm{i}A|A|^{-1}K^* = 0, \tag{4.39}$$

which implies that

$$B^{(0)'} = \left[\tfrac{1}{5}\kappa_r + \tfrac{1}{2}\mathrm{i}\,(\arg A)'\right] B^{(0)}. \tag{4.40}$$

Integration of the latter equation, using (4.33), gives

$$B^{(0)} = B_0^{(0)} \exp\left[\tfrac{1}{5}\kappa_r x_2^+ + \tfrac{1}{2}\mathrm{i}\arg(\mathrm{i}A)\right]. \tag{4.41}$$

Equations (4.32) and (4.41) show that (4.2) will match onto (3.23) provided the integration constant in (4.41) is given by $B_0^{(0)} = \bar{B}_\infty^\dagger |\bar{B}_0|/(\gamma|\bar{A}_0|)^{\frac{3}{5}}$. In fact, the subharmonic amplitude in the present stage is given, to the required order of accuracy, by the downstream asymptotic expansion (3.23) of the corresponding previous-stage solution, but with the linearly growing fundamental amplitude $\bar{A}$ replaced by the appropriately scaled strongly nonlinear-critical-layer solution A, x_2 expressed in terms of x_2^+, and $\varkappa$ replaced by unity.

4.5. *The composite solution*

A uniformly valid composite solution, say $\mathscr{B}^{(c)}$, can be obtained for the entire parametric resonance stage by multiplying the subharmonic amplitude functions (3.2) and (4.2) and dividing by their common part which, apart from the appropriate gauge function, is given by (3.23). After some manipulation, this composite solution becomes

$$\mathscr{B}^{(c)} = \frac{\delta|\bar{B}_0|}{(\gamma|\bar{A}_0|)^{\frac{4}{5}}} \bar{B}^\dagger(\bar{x}) \exp\left[\sigma^{-\frac{3}{2}}\Phi(x_2^+) + \tfrac{1}{2}\mathrm{i}\arg A(x_2^+) - 4\mathrm{e}^{\frac{1}{4}\bar{x}} - \tfrac{1}{2}\mathrm{i}X_0\right], \tag{4.42}$$

where $\bar{B}^\dagger$ and $\bar{x}$ are given by (B 3) and (B 1), respectively.

5. Fully coupled stage

The continued growth of the subharmonic throughout the nonlinear-fundamental stage, cf. (4.2), (4.32) and (4.41), implies that the subharmonic will become large enough to affect the fundamental. This occurs when $\mathscr{B} = O(\sigma^{\frac{11}{2}})$, i.e. in view of (4.2), when $\Phi(x_2^+) = O(\Delta)$, where

$$\Delta = \sigma^{\frac{3}{2}} \ln(\sigma^{\frac{67}{10}}/\delta), \tag{5.1}$$

and leads to a new, fully coupled stage of evolution in which the subharmonic is influenced by both parametric-resonance and self-interaction effects. Since the subharmonic growth rate is asymptotically large on the x_2^+ scale, this stage first emerges while x_2^+ is still $O(1)$. The present analysis assumes that x_2^+ is at least $O(1)$ in the fully coupled stage, which requires that Δ be $O(1)$. Equation (5.1) then determines the corresponding upper limit on the initial subharmonic amplitude scaling δ.

Since the back-reaction of the subharmonic on the fundamental causes the latter to evolve on the same streamwise scale as the former, the appropriate streamwise lengthscale for this region is

$$x_1 = \sigma^{-\frac{3}{2}}(x_2^+ - \xi_s) = \sigma^{\frac{5}{2}}x + \sigma^{-\frac{3}{2}}(6\kappa_r^{-1}\ln\sigma - \xi_s), \tag{5.2}$$

where ξ_s is determined by $\Phi(\xi_s) = \Delta$. The fundamental and subharmonic critical-layer thicknesses will then both be $O(\sigma^{\frac{5}{2}})$ and (4.7) is, therefore, the relevant transverse coordinate. The appropriate amplitude scaling for this stage is

$$\mathscr{A} = \sigma^7 \tilde{A}(x_1)\mathrm{e}^{-\mathrm{i}X_0}, \qquad \tilde{A} = O(1), \tag{5.3}$$

$$\mathscr{B} = \sigma^{\frac{11}{2}} \tilde{B}(x_1)\mathrm{e}^{-\mathrm{i}X_0/2}, \qquad \tilde{B} = O(1), \tag{5.4}$$

with the spanwise-variable mean-flow change, $\mathrm{Re}\,[\mathrm{e}^{\mathrm{i}2Z}\mathscr{G}(x_1, y)]$, now being of the same order as the subharmonic instability wave that produced it. To account for the shorter

streamwise lengthscale of the amplitude variation, the streamwise wavenumbers (2.15) and (2.16) are now written as

$$\alpha_0 = \sigma\left[\bar{\alpha} - \sigma^{\frac{3}{2}}\mathrm{i}\left(\ln\tilde{A}\right)'\right], \tag{5.5}$$

$$\alpha_1 = \sigma\left[\bar{k}\cos\theta - \sigma^{\frac{3}{2}}\mathrm{i}\left(\ln\tilde{B}\right)'\right], \tag{5.6}$$

where the prime denotes differentiation with respect to x_1.

The appropriate inviscid Tollmien solutions are given by (2.19) and (2.20) with $r = \frac{3}{2}$ and $a_n^{\pm} \neq 0$ since the wave-interaction effects now produce both fundamental and subharmonic critical-layer velocity jumps at $O(\sigma^{\frac{3}{2}})$. Matching with the flow in the main-boundary-layer region then shows that the leading-order velocity jumps for the fundamental and subharmonic are given by

$$a_0^+ - a_0^+ = 2\mathrm{i}\left(\lambda_0/\bar{S}\right)^{\frac{1}{2}}\left(\ln\tilde{A}\right)', \tag{5.7}$$

$$a_1^+ - a_1^+ = \tfrac{5}{2}\mathrm{i}\left(\lambda_0/\bar{S}\right)^{\frac{1}{2}}\left(\ln\tilde{B}\right)'. \tag{5.8}$$

The inner limits of the Tollmien-region solutions show that the critical-layer flow expands like

$$u = \sigma\left[\bar{c} + \sigma^{\frac{3}{2}}\lambda_w\tilde{\eta} + \sigma^3 u^{(1)} + \sigma^{\frac{9}{2}}u^{(2)} + \sigma^6 u^{(3)} + \sigma^{\frac{15}{2}}u^{(4)} + \ldots\right], \tag{5.9}$$

$$v = \sigma^{\frac{15}{2}}\left[\mathrm{Re}\left(-\mathrm{i}\bar{\alpha}\lambda_0 Y_c\tilde{B}\mathrm{e}^{\mathrm{i}X^+/2}\right)\cos Z + \sigma^{\frac{3}{2}}v^{(2)} + \sigma^3 v^{(3)} + \ldots\right], \tag{5.10}$$

$$w = \sigma^4\left[w^{(1)} + \sigma^{\frac{3}{2}}w^{(2)} + \sigma^3 w^{(3)} + \ldots\right], \tag{5.11}$$

$$p = \sigma^{\frac{13}{2}}\left[\mathrm{Re}\left(\tfrac{1}{2}\lambda_0\bar{c}\tilde{B}\mathrm{e}^{\mathrm{i}X^+/2}\right)\cos Z + \sigma^{\frac{3}{2}}p^{(2)} + \sigma^3 p^{(3)} + \ldots\right], \tag{5.12}$$

where the $u^{(l)}$, $v^{(l)}$, $w^{(l)}$, and $p^{(l)}$ are functions of X^+, x_1, $\tilde{\eta}$ and Z.

Integrating the fundamental component of $\partial u^{(4)}/\partial\tilde{\eta}$ and the subharmonic component of $\partial u^{(3)}/\partial\tilde{\eta}$ across the critical layer, and using the leading-order term in (2.21), produces expressions for the velocity jumps $a_0^+ - a_0^+$ and $a_1^+ - a_1^+$ that can be combined with the corresponding expressions obtained from the flow outside the critical layer, i.e. (5.7) and (5.8), to obtain the following matching conditions:

$$\frac{1}{\pi}\int_0^{2\pi}\int_{-\infty}^{+\infty}\frac{\partial u^{(4)}}{\partial\tilde{\eta}}\mathrm{e}^{-\mathrm{i}X^+}\mathrm{d}\tilde{\eta}\mathrm{d}X^+ = 2\mathrm{i}\left(\lambda_0/\bar{S}\right)^{\frac{1}{2}}\tilde{A}', \tag{5.13}$$

$$\frac{1}{2\pi}\int_0^{4\pi}\int_{-\infty}^{+\infty}\frac{\partial u^{(3)}}{\partial\tilde{\eta}}\mathrm{e}^{-\mathrm{i}X^+/2}\mathrm{d}\tilde{\eta}\mathrm{d}X^+ = 5\mathrm{i}\left(\lambda_0/\bar{S}\right)^{\frac{1}{2}}\tilde{B}'\cos Z. \tag{5.14}$$

Substituting (5.9)–(5.12) into the continuity and momentum equations produces a coupled set of equations that determine the $u^{(l)}$, $v^{(l)}$, $w^{(l)}$, and $p^{(l)}$. Not surprisingly, these equations are the same as the corresponding equations in G&L, i.e. their (5.14)–(5.21), but with their $\bar{\eta}$, $\bar{\gamma}$, A_0, A, U_0', and λ replaced by $\tilde{\eta}$, $\bar{k}$, $\tilde{A}$, $\frac{1}{2}\tilde{B}$, λ_0, and σ^9/R, respectively. The streamwise scale is shorter and the critical-layer thickness is larger than in the G&L analysis, but this only changes the transverse boundary conditions, which are obtained by matching the critical-layer solutions with the inviscid-Tollmien-layer solutions. The altered boundary conditions produce a reordering of the terms associated with the basic flow *vis-à-vis* those of the G&L analysis. The net result is a shift of the linear-growth terms to higher-order problems, which means that

the relevant amplitude evolution equations can be obtained by simply dropping the linear-growth terms from the corresponding equations given in G&L, i.e. their (5.50) and (5.51). (The G&L amplitude equations have also been derived in a different context by Wu 1992.) In the present notation, these equations become

$$\frac{1}{\kappa_r^4\gamma}\tilde{A}' = -\mathrm{i}M\int_{-\infty}^{x_1}\int_{-\infty}^{\xi_1}\left[2(x_1-\xi_1)^3\tilde{A}(\xi_1)\tilde{B}(\xi_2)\tilde{B}^*(2\xi_1+\xi_2-2x_1)\right.$$
$$\left.+K_2\tilde{B}(\xi_1)\tilde{A}(\xi_2)\tilde{B}^*(\xi_1+2\xi_2-2x_1)\right]\mathrm{d}\xi_2\mathrm{d}\xi_1$$
$$+\tfrac{1}{10}\mathrm{i}M^2\int_{-\infty}^{x_1}\int_{-\infty}^{\xi_1}\int_{-\infty}^{\xi_2}K_3\tilde{B}(\xi_1)\tilde{B}(\xi_2)\tilde{B}(\xi_3)\tilde{B}^*(\xi_1+\xi_2+\xi_3-2x_1)\mathrm{d}\xi_3\mathrm{d}\xi_2\mathrm{d}\xi_1, \tag{5.15}$$

$$\frac{1}{\kappa_r^4\gamma}\tilde{B}' = 4\mathrm{i}\int_{-\infty}^{x_1}(x_1-\xi_1)^2\tilde{A}(\xi_1)\tilde{B}^*(2\xi_1-x_1)\mathrm{d}\xi_1$$
$$+\mathrm{i}M\int_{-\infty}^{x_1}\int_{-\infty}^{\xi_1}K_1\tilde{B}(\xi_1)\tilde{B}(\xi_2)\tilde{B}^*(\xi_1+\xi_2-x_1)\mathrm{d}\xi_2\mathrm{d}\xi_1, \tag{5.16}$$

where

$$K_1(x_1|\xi_1,\xi_2) = \tfrac{1}{10}(x_1-\xi_1)\left[2(x_1-\xi_1)^2-(x_1-\xi_1)(x_1-\xi_2)+3(x_1-\xi_2)^2\right], \tag{5.17}$$
$$K_2(x_1|\xi_1,\xi_2) = (x_1-\xi_1)(x_1-\xi_2)(2x_1-\xi_1-\xi_2), \tag{5.18}$$
$$K_3(x_1|\xi_1,\xi_2,\xi_3) = \tfrac{1}{4}(x_1-\xi_1)\{(x_1+\xi_1+\xi_2-3\xi_3)(x_1-\xi_2)(x_1-2\xi_1+\xi_2)$$
$$-(x_1+\xi_1-2\xi_2)\left[(x_1+\xi_1-2\xi_2)^2-3(x_1-\xi_2)^2\right]\}, \tag{5.19}$$

and $M = \frac{5}{8}\lambda_0^2(\lambda_0\bar{S})^{\frac{1}{3}}$. Substituting (5.2) into (4.1) and (4.2) and expanding the resulting expressions in the limit of $\sigma \to 0$ shows that matching with the nonlinear-fundamental region requires that the solutions to (5.15) and (5.16) satisfy the upstream conditions

$$\tilde{A} \to A(\xi_s), \tag{5.20}$$

$$\tilde{B} \to B^{(0)}(\xi_s)\mathrm{e}^{\Phi'(\xi_s)x_1}, \tag{5.21}$$

as $x_1 \to -\infty$, rather than those given in G&L. These conditions reflect the fact that both the fundamental amplitude and the subharmonic growth rate remain constant on the x_1 lengthscale in the upstream region, i.e. the nonlinear-fundamental region.

6. Rescaled equations

The strongly nonlinear critical-layer equations (4.11)–(4.13) can be used to determine the fundamental amplitude throughout the entire parametric-resonance stage because they reduce to the appropriate linear equations, (3.9), (3.10) and (3.15), as $x_2^+ \to -\infty$. These equations and the composite solution (4.42) for the subharmonic can be rescaled to minimize the number of parameters by introducing the variables

$$\bar{x}^+ = \kappa_r x_2^+ + \ln(\Upsilon|\bar{A}_0|), \tag{6.1}$$

$$\bar{X} = X^+ + \arg\bar{A}_0 + \kappa_i x_2^+, \tag{6.2}$$

$$\bar{Y} = (\lambda_0^2\eta + \kappa_i)/\kappa_r, \tag{6.3}$$

$$\mathscr{A}^\dagger = \Upsilon A\exp\left[-\mathrm{i}\left(\arg\bar{A}_0 + \kappa_i x_2^+\right)\right], \tag{6.4}$$

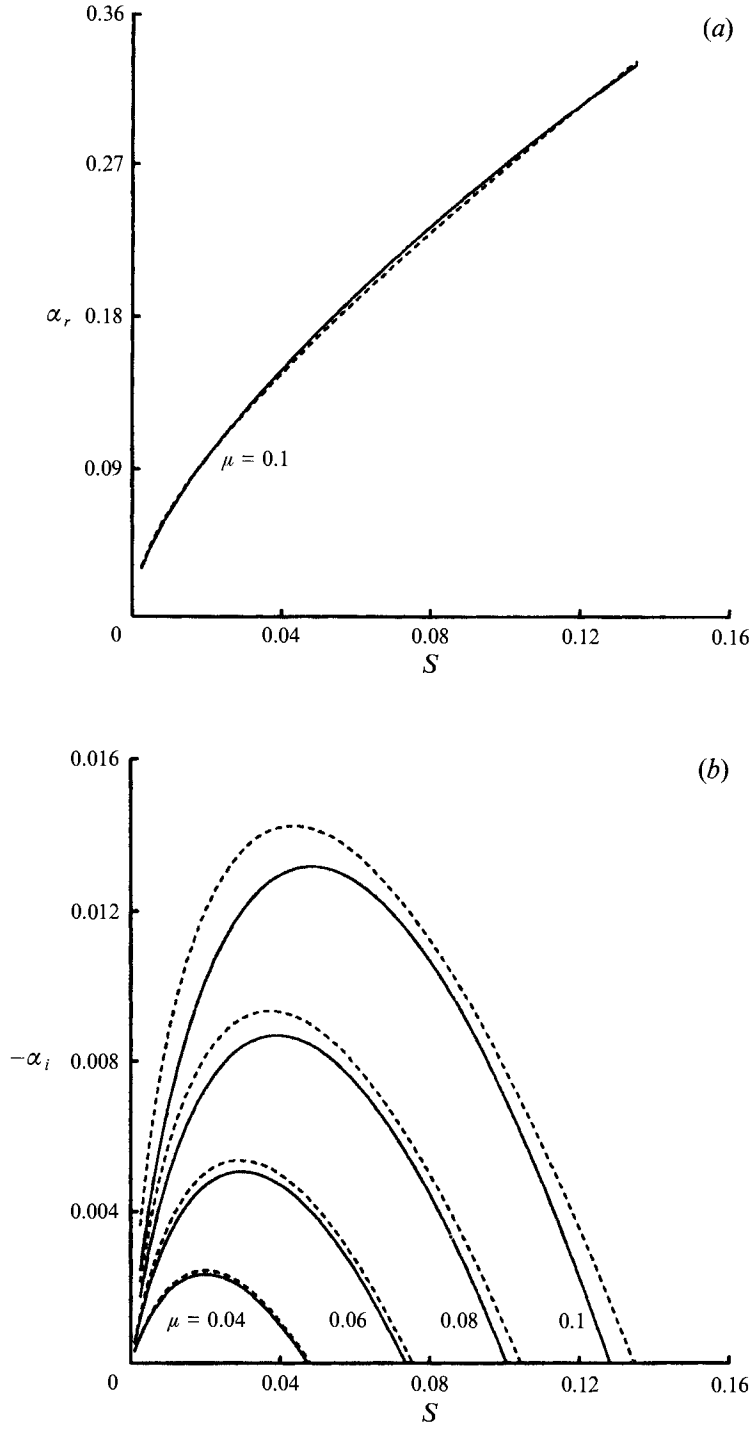

FIGURE 2. Wavenumber *vs.* frequency for a Falkner–Skan boundary-layer flow at various values of μ. Solid lines, exact solutions; dashed lines, asymptotic solutions.

$$Q = \frac{\lambda_0^2}{\kappa_r \bar{\mu}_c} \frac{\partial u_0^{(2)}}{\partial \eta}, \tag{6.5}$$

$$\mathscr{B}^\dagger = \frac{\bar{B}_\infty^\dagger \mathscr{B}^{(c)}(\bar{x}^+)}{\mathscr{B}^{(c)}(\bar{x}^+ = 0)} \exp\left[\mathrm{i}\left(-\tfrac{1}{2}\kappa_i \kappa_r^{-1} \bar{x}^+ + \tfrac{1}{4}\pi\right)\right], \tag{6.6}$$

where $\Upsilon = \lambda_0 \bar{\alpha}^3 / \bar{S} \kappa_r^2$ and $\mathscr{A}^\dagger$ turns out to be purely real. Equations (4.11) and (4.13) along with the upstream-matching condition (4.14) then become

$$\left(\frac{\partial}{\partial \bar{x}^+} + \bar{Y}\frac{\partial}{\partial \bar{X}} + \mathscr{A}^\dagger \sin \bar{X} \frac{\partial}{\partial \bar{Y}} - \frac{1}{\bar{R}} \frac{\partial^2}{\partial \bar{Y}^2}\right) Q = -\mathscr{A}^\dagger \sin \bar{X}, \tag{6.7}$$

$$\frac{1}{\pi} \int_{-\infty}^{+\infty} \int_0^{2\pi} Q \sin \bar{X} \mathrm{d}\bar{X} \mathrm{d}\bar{Y} = -\pi \frac{\mathrm{d}\mathscr{A}^\dagger}{\mathrm{d}\bar{x}^+}, \tag{6.8}$$

and

$$\mathscr{A}^\dagger \to \mathrm{e}^{\bar{x}^+} \quad \text{as} \quad \bar{x}^+ \to -\infty. \tag{6.9}$$

The uniformly valid composite solution for the subharmonic amplitude (4.42) becomes

$$\mathscr{B}^\dagger = \varrho^{\frac{1}{3}} \bar{B}^\dagger(\bar{x}) \exp\left(\varrho^{-\frac{1}{4}} \int_0^{\bar{x}^+} \mathscr{A}^{\dagger\frac{1}{4}} \mathrm{d}\xi - 4\mathrm{e}^{\frac{1}{4}\bar{x}}\right), \tag{6.10}$$

where $\varrho = \sigma^6 \Upsilon / \gamma$ and it follows from (4.4), (6.1) and (B 1) that

$$\bar{x} = \bar{x}^+ - \ln \varrho. \tag{6.11}$$

The solutions to (6.7) and (6.8) must match with the 'outer' flow in the inviscid Tollmien region, which requires that Q be periodic in $\bar{X}$ and satisfy the homogeneous boundary condition $Q \to 0$ as $\bar{Y} \to \pm\infty$. This strongly nonlinear critical-layer problem is solved using the numerical procedure given in Goldstein & Hultgren (1988) and the reader is referred to that paper for details of the method. The analytic solution (B 9) with $\varkappa$ replaced by unity is used to determine the function $\bar{B}^\dagger$ in the composite solution (6.10).

7. Results and discussion

Figure 2 is a comparison of the (complex) wavenumber α predicted by the long-wavelength/weak-adverse-pressure-gradient asymptotic solution to that determined from a corresponding numerical solution to the Rayleigh stability problem. The curves correspond to a Falkner–Skan boundary layer in which case the first correction to the wall-shear stress λ_1 is 1.2989 and the base-flow vorticity gradient at the critical level $\bar{\mu}_c$ is $\bar{\mu} - (\frac{1}{2} + \sigma^2 \bar{\mu})\bar{c}^2$. The dashed curves correspond to the asymptotic solution. The first three terms in (2.22) were used to compute the real part of the wavenumber in figure 2(*a*). This gives a good approximation to the exact solution at $\mu = 0.1$, which is somewhat greater than half the value of μ at separation. It is necessary to include $O(\sigma^2)$ terms in κ_r in order to obtain similar agreement for the imaginary part of the wavenumber, $\alpha_i = -\sigma^4 \kappa_r$. This can easily be done, for the Falkner–Skan profile, by extending the outer linear solution to higher order. The resulting expression for κ_r is just (3.18) but with λ_0 replaced by $\lambda_0 - \sigma^2 \lambda_1$ and

$$\sigma^2 \left(3 + \tfrac{1}{4}J_1^2 - 3J_1 - 2J_2\right) \bar{S} / \lambda_0$$

added to M_0. The resulting approximation for κ_r produces the best results when left as a rational function of σ. Figure 2(*b*) shows that this approximation is reasonably good even when $\mu = 0.1$.

The rescaled fundamental amplitude $\mathscr{A}^\dagger$ depends only on the rescaled critical-layer Reynolds number $\bar{R}$, which characterizes the ratio of inertia to viscous-diffusion effects in the critical layer. Figure 3(*b*) shows that the growth rate of the fundamental drops off sharply and decreases towards zero once nonlinearity comes into play. As in the shear-layer analyses of Goldstein & Hultgren (1988) and Hultgren (1992), the presence of viscosity, no matter how small, counteracts the inviscid roll-up of vorticity (cf. Goldstein & Leib 1988) and eventually leads to a slow algebraic growth of $\mathscr{A}^\dagger$ with increasing $\bar{x}^+/\bar{R}$.

The rescaled subharmonic amplitude $\mathscr{B}^\dagger$ not only depends on $\bar{R}$ but also on $\bar{\kappa}_i$ which characterizes the effective wavenumber detuning (see (B 7)), ψ which characterizes the effective initial phase difference between the subharmonic and the fundamental (see (B 8)), and the small parameter ϱ, $\propto$ (pressure gradient)^3, which characterizes the ratio of the fundamental amplitude in the initial parametric-resonance stage to that in the nonlinear-fundamental stage and, therefore, determines the distance on the $\bar{x}^+$ scale between these two stages, cf. (6.11). The rescaled subharmonic amplitude $\mathscr{B}^\dagger$ and growth rate $\mathrm{Re}(\mathscr{B}^{\dagger\prime}/\mathscr{B}^\dagger)$ are plotted in figures 3–5 for various values of $\bar{R}$, $\bar{\kappa}_i$ and ψ, with $\varrho = 0.05$ which approximates the value of ϱ for the most rapidly growing fundamental in a Falkner–Skan boundary-layer flow with $\mu = 0.08$. These figures show that the parametric resonance is initiated at a relatively short distance (on the $\bar{x}^+$ scale) upstream of the location where the fundamental becomes nonlinear. The initial subharmonic amplitude scaling δ is left unspecified throughout the entire parametric-resonance stage (apart from the restriction given in §5) because the subharmonic is determined by linear equations there. The vertical distance between the fundamental and subharmonic curves in figures 3(*a*), 4 and 5 is, therefore, arbitrary.

Since the instability waves are initially non-interacting, the subharmonic grows in accordance with linear theory until the fundamental amplitude becomes large enough for the parametric resonance to come into play. This happens while the fundamental instability wave is still linear and occurs when the fundamental component of the transverse velocity fluctuation is of the order of the linear growth rate raised to the $\frac{7}{2}$ power. In the Craik (1971) analysis, which applies to Tollmien–Schlichting waves at finite Reynolds numbers, the initial wave interaction occurs when the fundamental amplitude is of the order of the linear growth rate. Mankbadi *et al.* (1993), who consider an appropriate large-Reynolds-number limit of the Craik (1971) problem, find that the initial interaction occurs when the fundamental component of the transverse velocity fluctuation is of the order of the linear growth rate raised to the $\frac{11}{4}$ power. These differences arise because the wave interaction takes place within a non-equilibrium (or growth-dominated) critical layer in the present analysis rather than throughout the external flow as in the Craik (1971) analysis or within an equilibrium (or viscosity-dominated) critical layer as in the Mankbadi *et al.* (1993) analysis.

Depending on the values of $\bar{\kappa}_i$ and ψ (figures 4 and 5), the parametric-resonance effects may either enhance or reduce the initial subharmonic growth rate, but always lead to an increase in the subharmonic growth rate, proportional to the quarter power of the local fundamental amplitude, sufficiently far downstream, cf. (3.23). The Craik (1971) and Mankbadi *et al.* (1993) solutions also exhibit faster than exponential growth in the parametric-resonance stage, but with the growth rate increasing in direct proportion to the fundamental amplitude. Section B.2 of Appendix B shows how the exponential growth of the fundamental can convert an equilibrium critical layer of

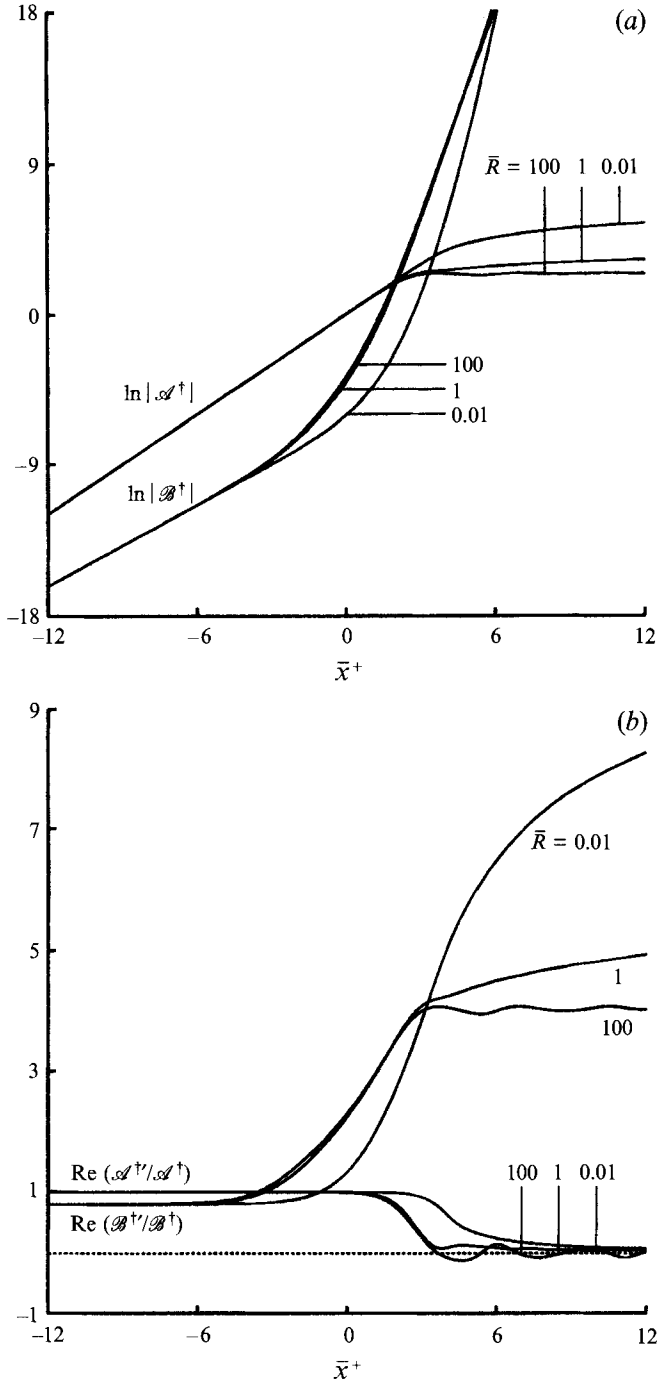

FIGURE 3. Scaled fundamental and subharmonic amplitudes *vs.* shifted long streamwise scale for $\bar{\kappa}_i = 0$, $\psi = \frac{1}{4}\pi$, $\varrho = 0.05$ and various values of $\bar{R}$.

the type that appears in the Mankbadi *et al.* (1993) analysis into a non-equilibrium critical layer of the type considered herein (see Goldstein 1994 for a detailed discussion of this issue).

The subharmonic continues to grow as an exponential of an exponential until

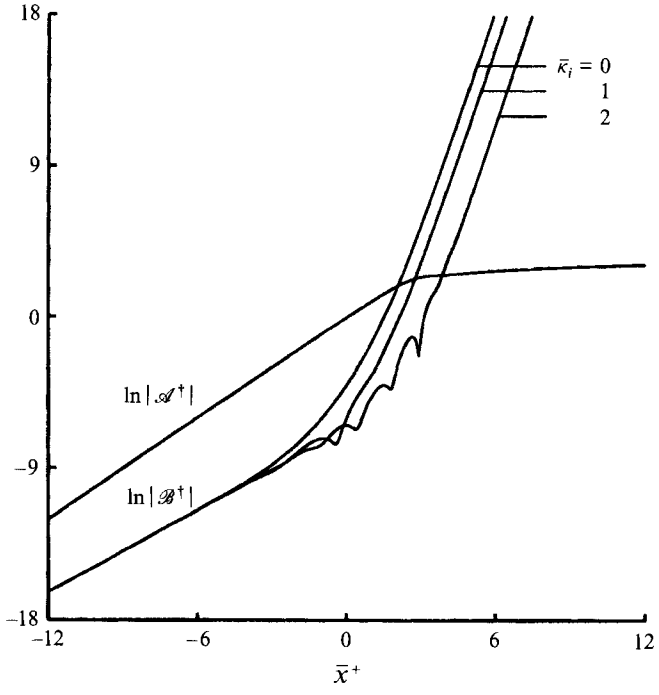

FIGURE 4. Scaled fundamental and subharmonic amplitudes *vs.* shifted long streamwise scale for $\bar{R} = 1$, $\psi = \frac{1}{4}\pi$, $\varrho = 0.05$ and various values of $\bar{\kappa}_i$.

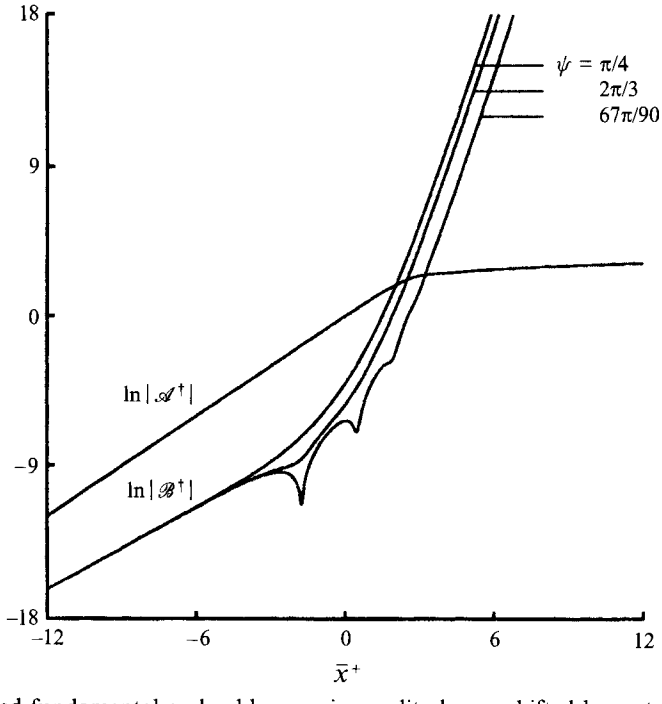

FIGURE 5. Scaled fundamental and subharmonic amplitudes *vs.* shifted long streamwise scale for $\bar{R} = 1$, $\bar{\kappa}_i = 0$, $\varrho = 0.05$ and various values of ψ.

nonlinear self-interaction effects alter the growth rate of the fundamental. This occurs when the fundamental component of the transverse velocity fluctuation is of the order of the linear growth rate squared. The subharmonic evolution is then controlled by parametric-resonance effects and occurs over a streamwise lengthscale that is short compared to the scale on which the fundamental evolves but still long compared to a wavelength. The continual increase in the subharmonic growth rate is then reduced and eventually becomes algebraic once the fundamental critical layer ages into a quasi-equilibrium stage (figure 3*b*). This assumes, of course, that the fully coupled stage does not come into play before the fundamental reaches its quasi-equilibrium stage.

Figure 3 shows the rescaled subharmonic amplitude and growth rate for several values of the parameter $\bar{R}$. This parameter affects the subharmonic solution through the usual viscous-diffusion terms in the initial parametric-resonance stage but only indirectly through the fundamental amplitude in the nonlinear-fundamental stage, since the subharmonic critical layer is strictly inviscid there. Decreasing $\bar{R}$, therefore, affects the composite solution (6.10) in two ways. First, the initiation of the parametric resonance is delayed because a larger fundamental amplitude is required for the parametric-resonance effects to balance the increasing viscous-diffusion effects (figure 3*a*); and second, the final subharmonic growth rate is enhanced because of the increasing saturation level of the fundamental amplitude (figure 3*b*). Note that the subharmonic growth rate appears to oscillate about a constant value for the largest value of $\bar{R}$ shown in figure 3, which gives the impression that the subharmonic is again growing exponentially. However, the fundamental amplitude has not yet reached its quasi-equilibrium stage in this particular case. Once this occurs, the subharmonic growth rate again will exhibit the slow algebraic increase evident in the other curves.

Figures 4 and 5 show the rescaled subharmonic amplitude for various values of the parameters $\bar{\kappa}_i$ and ψ. These parameters only affect the solution in the initial parametric-resonance stage, i.e. they only influence $\bar{B}^{\dagger}(\bar{x})$. G&L show that $\bar{\kappa}_i$ and ψ alter the development of the subharmonic by changing the direction of energy exchange between the subharmonic and fundamental. This effect is responsible for the oscillations in figures 4 and 5. G&L also find that the energy transfer to the subharmonic is maximized when $\bar{\kappa}_i = 0$ and $\psi = \frac{1}{4}\pi$. This result, also evident in figures 4 and 5, implies that detuning delays the ultimate subharmonic amplification produced by the parametric resonance (see §B.3 of Appendix B) and thereby gives the fundamental more 'time' to reach its nonlinear saturation amplitude.

The fully coupled stage occurs when the subharmonic amplitude becomes $O(\sigma^{\frac{11}{2}})$, which is larger than the $O(\sigma^{10})$ scaling of the G&L analysis. The difference is due to the thicker critical layer in which the present interaction takes place. The instability-wave amplitudes can be made parameter independent in the fully coupled stage by introducing the rescaled variables

$$\bar{x}_1 = \Phi'(\xi_s)x_1 - \ln\left[\Phi'(\xi_s)|A(\xi_s)|^{\frac{1}{2}}/M^{\frac{1}{2}}|B^{(0)}(\xi_s)|\right], \tag{7.1}$$

$$\tilde{A}^{\dagger} = 10\tilde{A}/A(\xi_s), \tag{7.2}$$

$$\tilde{B}^{\dagger} = A(\xi_s)^{\frac{1}{2}}\tilde{B}/M^{\frac{1}{2}}\Phi'(\xi_s), \tag{7.3}$$

where $\tilde{A}^{\dagger}$ is defined so that the amplitude evolution equations (5.15) and (5.16) reduce exactly to (5.51) and (5.50) of G&L less the linear-growth terms. The initial conditions (5.20) and (5.21) are then

$$\tilde{A}^{\dagger} \to 10, \tag{7.4}$$

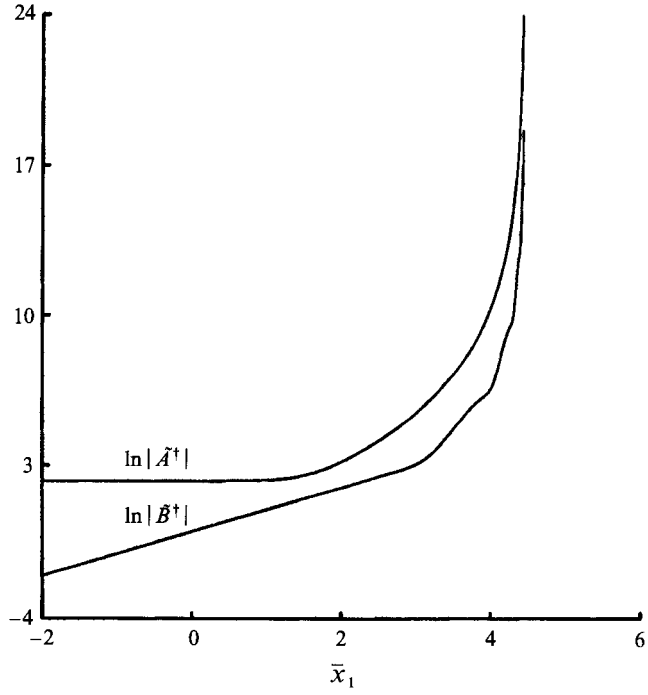

FIGURE 6. Scaled fundamental and subharmonic amplitudes *vs.* long streamwise scale in the fully coupled stage.

$$\tilde{B}^\dagger \to e^{i\frac{\pi}{4}} e^{\bar{x}_1}, \tag{7.5}$$

as $\bar{x}_1 \to -\infty$. The computed solutions for $\tilde{A}^\dagger$ and $\tilde{B}^\dagger$ are shown in figure 6. They were determined by using the numerical procedure given in G&L. As in G&L, the self-interaction of the subharmonic produces a further enhancement of its growth and ultimately leads to a singularity at a finite downstream position, which now occurs much more abruptly due to the shorter streamwise scale, cf. (5.2). This explosive growth is then transferred to the fundamental through the mutual-interaction and back-reaction effects.

G&L derive local asymptotic solutions valid in the neighborhood of the singularity. Those results, given by their (6.1)–(6.8), also apply to the present singularity and suggest that the analysis will break down at an $O(\sigma^{\frac{3}{2}})$ x_1-scale distance upstream of the singularity. The critical layer then expands to fill the inviscid Tollmien wall layer which therefore becomes fully nonlinear while the instability wave amplitudes are still small. The next stage of evolution will be governed by the three-dimensional, unsteady 'triple deck' equations, but with the viscous terms deleted.

The authors wish to thank Dr Sang Soo Lee for many stimulating discussions and advice on adapting the G&L numerical code to the fully coupled problem of the present study.

Appendix A. Solution of (3.11) and (3.12)

Equations (3.9)–(3.12) imply that

$$\bar{u}_1^{(0)} = \mathrm{Re}\left(\hat{\bar{u}}_1^{(0)} e^{iX/2}\right), \tag{A 1}$$

$$\bar{v}_1^{(2)} = \mathrm{Re}\left(\hat{\bar{v}}_{1,1}^{(2)} e^{iX/2} + \hat{\bar{v}}_{1,3}^{(2)} e^{i3X/2}\right), \tag{A 2}$$

and it follows that only the $\hat{\bar{v}}_{1,1}^{(2)}$ term in (A 2) contributes to the velocity jump condition (3.16). Substituting (A 1) and (A 2) into (3.11) and (3.12) and taking the transverse Fourier transform, defined by

$$\mathscr{F} = \frac{1}{2\pi}\int_{-\infty}^{+\infty} d\eta e^{-i\xi\eta}, \tag{A 3}$$

leads to two equations for the subharmonic that can be written in the following forms:

$$\tilde{\mathscr{L}}_2 \tilde{U}(x_2, \xi) = \tfrac{3}{4} i\lambda_0 \bar{S} \bar{B}(x_2) e^{-f(\xi)} H'(-\xi), \tag{A 4}$$

$$\tilde{\mathscr{L}}_2 \tilde{Q}(x_2, \xi) = \tfrac{1}{2}\bar{\alpha}\bar{S}\left[\bar{\mu}_c \bar{B}(x_2) e^{-f(\xi)} H'(-\xi) - \bar{A}(x_2)\xi^2 \tilde{U}^*(x_2, -\xi) e^{-2f(\xi)}\right], \tag{A 5}$$

where

$$\tilde{\mathscr{L}}_2 = \bar{c}\frac{\partial}{\partial x_2} - \tfrac{1}{2}\bar{\alpha}\lambda_0 \frac{\partial}{\partial \xi}, \tag{A 6}$$

$$f(\xi) = 2\xi^3/3\bar{\alpha}\lambda_0 R, \tag{A 7}$$

$\tilde{U}\exp(f)$ and $\tilde{Q}\exp(f)$ are the Fourier transforms of $\hat{\bar{u}}_1^{(0)}$ and $\partial^2 \hat{\bar{v}}_{1,1}^{(2)}/\partial\eta^2$, respectively, H is the Heaviside step function, and the asterisk denotes complex conjugation.

Integration of (A 4) along the characteristic

$$s_- = \bar{\alpha}\lambda_0 x_2/4\bar{c} - \xi/2 \tag{A 8}$$

of (A 6) shows that

$$\tilde{U}(x_2, \xi) = \tfrac{3}{2} i\bar{c}\bar{B}\left(x_2 + 2\bar{c}\xi/\bar{\alpha}\lambda_0\right) H(-\xi). \tag{A 9}$$

Substitution of this result into (A 5) and integration of the result along the s_- characteristic yields

$$\tilde{Q}(x_2, \xi) = \frac{\bar{S}}{\lambda_0}\left[\bar{\mu}_c \bar{B}\left(x_2 + \frac{2\bar{c}\xi}{\bar{\alpha}\lambda_0}\right) H(-\xi)\right.$$
$$\left. + \tfrac{3}{2} i\bar{c}\int_{\xi}^{+\infty} s^2 e^{-2f(s)} H(s) \bar{A}\left(x_2 + \frac{2\bar{c}}{\bar{\alpha}\lambda_0}(\xi - s)\right) \bar{B}^*\left(x_2 + \frac{2\bar{c}}{\bar{\alpha}\lambda_0}(\xi - 2s)\right) ds\right]. \tag{A 10}$$

The result (3.19) can now be obtained from the identity

$$\int_{-\infty}^{+\infty} \frac{\partial^2 \hat{\bar{v}}_{1,1}^{(2)}}{\partial\eta^2} d\eta = 2\pi \tilde{Q}(x_2, 0), \tag{A 11}$$

by performing a few relatively simple manipulations.

Appendix B. Analytic solution for $\bar{B}$

B.1. *The general case*

A convergent-series solution for $\bar{B}$ is obtained in this appendix. The manipulations are most easily carried out in terms of the rescaled variables

$$\bar{x} = \kappa_r x_2 + \ln(\gamma|\bar{A}_0|), \tag{B 1}$$

$$\bar{A}^\dagger = \gamma \bar{A} \exp\left[-i\left(\arg \bar{A}_0 + \kappa_i x_2\right)\right], \tag{B 2}$$

$$\bar{B}^{\dagger} = |\bar{B}_0|^{-1}(\gamma|\bar{A}_0|)^{\frac{4}{5}\varkappa}\bar{B}\exp\left[-\tfrac{1}{2}\mathrm{i}\left(\arg\bar{A}_0 + \kappa_i x_2\right)\right]. \tag{B 3}$$

After changing the variable of integration in (3.19) from ξ to $2(x_2-\xi)$, the amplitude-evolution equations, (3.17) and (3.19), and the associated initial condition, (3.22), become

$$\bar{A}^{\dagger} = \mathrm{e}^{\bar{x}}, \tag{B 4}$$

$$\bar{B}^{\dagger'} = \bar{\kappa}\bar{B}^{\dagger} + \tfrac{1}{2}\mathrm{i}\int_0^{\infty} s^2\mathrm{e}^{-s^3/48\bar{R}}\bar{A}^{\dagger}(\bar{x}-\tfrac{1}{2}s)\bar{B}^{\dagger *}(\bar{x}-s)\mathrm{d}s, \tag{B 5}$$

and

$$\bar{B}^{\dagger} \to \mathrm{e}^{\bar{\kappa}\bar{x}+\mathrm{i}\psi} \quad \text{as} \quad \bar{x} \to -\infty \tag{B 6}$$

where $\bar{\kappa} \equiv \frac{4}{5}\varkappa + \mathrm{i}\bar{\kappa}_i$. The rescaled subharmonic amplitude $\bar{B}^{\dagger}$ therefore depends on three real parameters: $\bar{R}$ which characterizes the ratio of inertia to viscous-diffusion effects;

$$\bar{\kappa}_i \equiv \left\{\tfrac{3}{10}\varkappa\left[\kappa_i - \left(\lambda_0\bar{S}\right)^{\frac{1}{2}}\chi\right] + \tfrac{1}{2}(\varkappa-1)\kappa_i\right\}\kappa_r^{-1}, \tag{B 7}$$

which characterizes the effective wavenumber detuning; and

$$\psi \equiv \arg\bar{B}_0 - \tfrac{1}{2}\arg\bar{A}_0 - \bar{\kappa}_i\ln(\gamma|\bar{A}_0|), \tag{B 8}$$

which characterizes the effective initial phase angle between the subharmonic and the fundamental.

Following G&L, the ansatz

$$\bar{B}^{\dagger} = \mathrm{e}^{\bar{\kappa}\bar{x}+\mathrm{i}\psi}\sum_{n=0}^{\infty} g_n\mathrm{e}^{2n\bar{x}} + \mathrm{i}\mathrm{e}^{\bar{\kappa}^*\bar{x}-\mathrm{i}\psi}\sum_{n=0}^{\infty} h_n^*\mathrm{e}^{(2n+1)\bar{x}} \tag{B 9}$$

is substituted into (B 5) and like powers of $\mathrm{e}^{\bar{x}}$ are equated to obtain the recursion relations

$$g_{n+1} = \frac{e_{2n+1}}{2(n+1)(2n+1+q)^3}h_n, \tag{B 10}$$

$$h_n = \frac{e_{2n}}{2(n+p)(2n+q)^3}g_n, \tag{B 11}$$

where $g_0 = 1$ and $h_0 = e_0/2pq^3$, $p \equiv \frac{1}{2} + \mathrm{i}\bar{\kappa}_i$, $q \equiv \frac{1}{2} + \bar{\kappa}$,

$$e_n \equiv \tfrac{1}{2}(n+q)^3\int_0^{\infty} s^2\exp\left[-s^3/48\bar{R} - (n+q)s\right]\mathrm{d}s$$

$$= \begin{cases} 8\pi\bar{R}(n+q)^3\mathrm{Hi}''\left(-(16\bar{R})^{\frac{1}{3}}(n+q)\right) & \text{for } \bar{R} \neq \infty \\ 1 & \text{for } \bar{R} = \infty \end{cases}, \tag{B 12}$$

and Hi denotes the Airy function integral defined on p. 448 of Abramowitz & Stegun (1964). Equations (B 10) and (B 11) are easily summed to obtain

$$g_n = \frac{1}{2^{2n}n!(p)_n(q)_{2n}^3}\prod_{m=1}^{2n} e_{m-1}, \tag{B 13}$$

$$h_n = \frac{1}{2^{2n+1}n!(p)_{n+1}(q)_{2n+1}^3}\prod_{m=1}^{2n+1} e_{m-1}, \tag{B 14}$$

where $(z)_n \equiv \Gamma(z+n)/\Gamma(z)$ denotes the generalized factorial function and $\Gamma(z)$ denotes the gamma function.

Application of the ratio test shows that the two sums in (B 9) are absolutely convergent for all $\bar{x}$. They are mainly determined by their first few terms when $\bar{x} \ll -1$ but more terms rapidly become important as $\bar{x}$ increases. The moduli of the individual terms tend to increase with n until, as required by absolute convergence, a maximum is reached and the moduli of the succeeding terms decrease as n increases. It follows from the properties of the gamma and Airy functions that both sums have a sharp peak near $n = N \equiv [\frac{1}{2}e^{\frac{1}{4}\bar{x}}]$ in the limit as $\bar{x} \to \infty$. The dominant contribution to each sum then comes from terms in the immediate neighbourhood of this peak and can be determined by Laplace's method for sums (Bender & Orszag 1978, p. 304).

In this method, the summation is centred on the index of the peak term by introducing $j = n - N$, where $|j|$ remains small compared to $N^{\frac{2}{3}}$ but may take on values greater than $N^{\frac{1}{2}}$, and g_n and h_n are replaced by their large-n approximations which are obtained from (B 13) and (B 14) by using

$$\prod_{m=1}^{n} e_{m-1} = [1 + O(n^{-2})] \prod_{m=1}^{\infty} e_{m-1} \quad \text{as} \quad n \to \infty \tag{B 15}$$

together with Stirling's formula (Abramowitz & Stegun 1964, p. 257). Thus, the first sum in (B 9) becomes

$$\sum_{n=0}^{\infty} g_n e^{2n\bar{x}} \sim \left(\frac{8}{\pi}\right)^{\frac{1}{2}} G_\infty \exp\left(\frac{3-2p-6q}{8}\bar{x} + 4e^{\frac{1}{4}\bar{x}}\right) \sum_{j=-\varepsilon N}^{+\varepsilon N} \exp\left(-8j^2 e^{-\frac{1}{4}\bar{x}}\right) \tag{B 16}$$

as $\bar{x} \to \infty$, where $\varepsilon > 0$ characterizes the region of summation and

$$G_\infty \equiv 2^{p-4}\pi^{-2}\Gamma(p)\Gamma(q)^3 \prod_{m=1}^{\infty} e_{m-1} \tag{B 17}$$

is a complex constant that, in view of (B 12) and the definitions of p and q, depends only on $\bar{R}$ and $\bar{\kappa}_i$. The sum on the right-hand side of (B 16) is determined to leading order by extending the region of summation to ∞ and converting the result into a Riemann sum for the error function, i.e.

$$\sum_{j=-\varepsilon N}^{+\varepsilon N} \exp\left(-8j^2 e^{-\frac{1}{4}\bar{x}}\right) \sim \frac{1}{\sqrt{8}} e^{\frac{1}{8}\bar{x}} \int_{-\infty}^{+\infty} e^{-t^2} dt = \left(\frac{\pi}{8}\right)^{\frac{1}{2}} e^{\frac{1}{8}\bar{x}} \tag{B 18}$$

as $\bar{x} \to \infty$. Substituting (B 18) into (B 16) then yields

$$\sum_{n=0}^{\infty} g_n e^{2n\bar{x}} \sim G_\infty \exp\left(\frac{2-p-3q}{4}\bar{x} + 4e^{\frac{1}{4}\bar{x}}\right) \tag{B 19}$$

as $\bar{x} \to \infty$. An analogous procedure shows that the complex conjugate of the right-hand side of (B 19) describes the leading-order asymptotic behaviour of the second sum in (B 9). Substitution of these results into (B 9) shows that

$$\bar{B}^\dagger \sim \bar{B}^\dagger_\infty e^{i\frac{\pi}{4}} \exp\left(\tfrac{1}{5}\varkappa\bar{x} + 4e^{\frac{1}{4}\bar{x}}\right) \tag{B 20}$$

as $\bar{x} \to \infty$, where

$$\bar{B}^\dagger_\infty \equiv 2|G_\infty| \cos\left(\psi + \arg G_\infty - \tfrac{1}{4}\pi\right) \tag{B 21}$$

is a real constant that depends on $\bar{R}$, $\bar{\kappa}_i$ and ψ. Equation (B 20) is invalid when $\psi = \frac{3}{4}\pi - \arg G_\infty$, in which case the asymptotic behaviour of $\bar{B}^\dagger$ is determined by higher-order terms.

B.2. *The viscous limit of (B 5)*

The integrand of (B 5) becomes highly concentrated around $s = 0$ in the viscous limit $\bar{R} \to 0$. The rescaled subharmonic amplitude equation therefore reduces to the ordinary differential equation

$$\bar{B}^{\dagger\prime} = \bar{\kappa}\bar{B}^{\dagger} + 8\mathrm{i}\bar{R}\bar{A}^{\dagger}\bar{B}^{\dagger *}, \tag{B 22}$$

which differs from the equation obtained by Craik (1971) in that the parametric-resonance coefficient is purely imaginary. The leading-order term in the small-σ expansion of $\bar{B}^{\dagger}$ is all that is needed for the subsequent analysis so $\varkappa$ is replaced by unity. As is well known, the solution to (B 22) that satisfies (B 6) is

$$\bar{B}^{\dagger} = (4\bar{R})^{1-p}\,\Gamma(p)\mathrm{e}^{\frac{13}{10}\bar{x}+\mathrm{i}\psi}\mathrm{I}_{p-1}\left(8\bar{R}\mathrm{e}^{\bar{x}}\right) + \mathrm{i}\,(4\bar{R})^{1-p^*}\,\Gamma(p^*)\mathrm{e}^{\frac{13}{10}\bar{x}-\mathrm{i}\psi}\mathrm{I}_{p^*}\left(8\bar{R}\mathrm{e}^{\bar{x}}\right), \tag{B 23}$$

where $\mathrm{I}_{\nu}(z)$ denotes the modified Bessel function. It follows from the asymptotic behaviour of the Bessel functions for large values of their argument (Abramowitz & Stegun 1964, p. 377) that

$$\bar{B}^{\dagger} \sim \pi^{-\frac{1}{2}}|\Gamma(p)|\cos\left[\psi + \arg\Gamma(p) - \bar{\kappa}_i \ln\left(4\bar{R}\right) - \tfrac{1}{4}\pi\right]\mathrm{e}^{\mathrm{i}\frac{\pi}{4}}\exp\left(\tfrac{4}{5}\bar{x} + 8\bar{R}\mathrm{e}^{\bar{x}}\right) \tag{B 24}$$

as $\bar{x} \to \infty$ – which can also be obtained by applying Laplace's method to (B 9) after replacing g_n and h_n with their leading-order small-$\bar{R}$ behaviour.

Comparing (B 24) with (B 20) shows that the approximation (B 22) is not uniformly valid as $\bar{x} \to \infty$. In fact, keeping the next-order term in the small-$\bar{R}$ expansion of (B 5), shows that the next-order correction to the right-hand side of (B 22) is

$$-\tfrac{1}{2}\mathrm{i}\pi\left(16\bar{R}\right)^{\frac{4}{3}}\mathrm{Hi}(0)\bar{A}^{\dagger}\left(q^*\bar{B}^{\dagger *} - 8\mathrm{i}\bar{R}\bar{A}^{\dagger *}\bar{B}^{\dagger}\right), \tag{B 25}$$

which implies that (B 22) is only valid when $\bar{x} \ll -\frac{4}{3}\ln(16\bar{R})$. As $\bar{x}$ increases beyond this region, non-equilibrium effects become equal to and eventually exceed viscous-diffusion effects as a result of the exponential increase in the subharmonic growth rate produced by the parametric resonance. The subharmonic critical layer is then of the non-equilibrium type and the rescaled subharmonic amplitude is again given by (B 20), but with $\bar{B}^{\dagger}_{\infty}$ replaced by its small-$\bar{R}$ limit.

The transition between the large-$\bar{x}$ asymptotic behaviour (B 20) and that given by (B 24) takes place in the streamwise region $\bar{\tau} \equiv \bar{x} + \frac{4}{3}\ln(16\bar{R}) = O(1)$ where viscous-diffusion and non-equilibrium effects are of equal importance. As pointed out by Goldstein (1994), the relevant solution for the subharmonic amplitude will take on the WKBJ form

$$\bar{B}^{\dagger} = \epsilon^{-\frac{16}{5}}\mathrm{e}^{\mathrm{i}\frac{\pi}{4}}\bar{b}(\bar{\tau})\exp\left[\epsilon^{-1}\int_{-\infty}^{\bar{\tau}}\bar{g}(s)\mathrm{d}s\right], \tag{B 26}$$

$$\bar{b} = \bar{b}^{(0)} + \epsilon\bar{b}^{(1)} + \ldots \tag{B 27}$$

as $\epsilon \to 0$, where $\epsilon \equiv (16\bar{R})^{\frac{1}{3}}$, and $\bar{b}^{(0)}$ and $\bar{g}$ turn out to be purely real. Substituting (B 26) into (B 5), changing the variable of integration from s to ϵs, expanding the resulting integrand in a Taylor series about $\epsilon = 0$, and making use of the integral representation of Hi (Abramowitz & Stegun 1964, p. 448) leads to

$$\begin{aligned}\bar{b}' + (\epsilon^{-1}\bar{g} - \bar{\kappa})\bar{b} = {} & -\tfrac{1}{2}\pi\mathrm{e}^{\bar{\tau}}\mathrm{Hi}'''(-\bar{g})\bar{b}^{*\prime} \\ & + \tfrac{1}{4}\pi\mathrm{e}^{\bar{\tau}}\left[2\epsilon^{-1}\mathrm{Hi}''(-\bar{g}) - \mathrm{Hi}'''(-\bar{g}) - \mathrm{Hi}''''(-\bar{g})\bar{g}'\right]\bar{b}^* + O(\epsilon)\end{aligned} \tag{B 28}$$

as $\epsilon \to 0$, where the prime denotes differentiation with respect to the argument.

Substituting the expansion (B 27) into this equation and equating like powers of ϵ shows that

$$\bar{g} = \tfrac{1}{2}\pi e^{\bar{\tau}} \mathrm{Hi}''(-\bar{g}), \tag{B 29}$$

$$\bar{b}^{(1)} - \bar{b}^{(1)*} = \bar{b}^{(0)\prime}/\bar{g}' + \left[\left(\bar{\kappa} - \tfrac{1}{2}\right)(\ln \bar{g})' + \tfrac{1}{2}(\ln \bar{g}')'\right] \bar{b}^{(0)}/\bar{g}'. \tag{B 30}$$

Taking the complex conjugate of (B 30) and substituting the resulting expression for $\bar{b}^{(1)*}$ back into (B 30) leads to a differential equation for $\bar{b}^{(0)}$ which is easily integrated to obtain

$$\bar{b}^{(0)} = \bar{b}_0^{(0)} (\bar{g})^{\frac{3}{10}} (\bar{g}')^{\frac{1}{2}}, \tag{B 31}$$

where $\bar{b}_0^{(0)}$ is a real constant. It follows from (B 29) that

$$\int_{-\infty}^{\bar{\tau}} \bar{g}(s)\mathrm{d}s \to \begin{cases} \frac{1}{2}e^{\bar{\tau}} & \text{as } \bar{\tau} \to -\infty \\ 4e^{\frac{1}{4}\bar{\tau}} + \displaystyle\int_{-\infty}^{+\infty} \left(\bar{g} - e^{\frac{1}{4}\bar{\tau}}\right) \mathrm{d}\bar{\tau} & \text{as } \bar{\tau} \to +\infty \end{cases} \tag{B 32}$$

and, therefore, that the solution (B 26), (B 29) and (B 31) will match onto (B 24) as $\bar{\tau} \to -\infty$ if

$$\bar{b}_0^{(0)} = 2^{\frac{4}{5}} \pi^{-\frac{1}{2}} |\Gamma(p)| \cos\left[\psi + \arg \Gamma(p) - \bar{\kappa}_i \ln(4\bar{R}) - \tfrac{1}{4}\pi\right]. \tag{B 33}$$

Since (B 32) implies that

$$\bar{B}^{\dagger} \sim \tfrac{1}{2}\epsilon^{-\frac{16}{5}} \bar{b}_0^{(0)} \exp\left[\epsilon^{-1} \int_{-\infty}^{+\infty} \left(\bar{g} - e^{\frac{1}{4}\bar{\tau}}\right) \mathrm{d}\bar{\tau}\right] \exp\left(\tfrac{1}{5}\bar{\tau} + 4\epsilon^{-1} e^{\frac{1}{4}\bar{\tau}}\right) \tag{B 34}$$

as $\bar{\tau} \to +\infty$, the solution (B 26) clearly has the same downstream asymptotic behaviour as (B 20).

B.3. *The strongly detuned limit of (B 5)*

The solution for the subharmonic amplitude in the strongly detuned limit $|\bar{\kappa}_i| \to \infty$ behaves similarly to the highly viscous solution. The subharmonic critical layer is always of the non-equilibrium type in the strongly detuned limit but with the dynamics dominated by linear-growth effects when $\bar{x} \ll \ln \bar{\kappa}_i^4$ and by parametric-resonance effects when $\bar{x} \gg \ln \bar{\kappa}_i^4$. The linear solution (B 6) is the leading-order solution in the former region, while the solution in the latter region is again given by (B 20) but with $\bar{B}_{\infty}^{\dagger}$ replaced by its large-$\bar{\kappa}_i$ limit, i.e.

$$\bar{B}_{\infty}^{\dagger} \sim 2^{-\frac{1}{2}} \bar{\kappa}_i^{\frac{12}{5}} e^{-\frac{\pi}{2}|\bar{\kappa}_i|} \cos\left[\psi + 4\bar{\kappa}_i\left(\ln|\bar{\kappa}_i| + \tfrac{1}{4}\ln 2 + 1\right) \pm \tfrac{6}{5}\pi - \tfrac{1}{4}\pi\right] \tag{B 35}$$

for $\bar{\kappa}_i \gtrless 0$. Equation (B 35) shows that the amplitude of a strongly detuned subharmonic at the end of the initial parametric-resonance stage is, as would be expected, much smaller than the corresponding amplitude of its order-one $\bar{\kappa}_i$ counterpart.

REFERENCES

ABRAMOWITZ, M. & STEGUN, I. A. 1964 *Handbook of Mathematical Functions.* US National Bureau of Standards.

BENDER, C. M. & ORSZAG, S. A. 1978 *Advanced Mathematical Methods for Scientists and Engineers.* McGraw–Hill.

BENNEY, D. J. & GUSTAVSSON, L. H. 1981 A new mechanism for linear and nonlinear hydrodynamic instability. *Stud. Appl. Maths* **64**, 185-209.

BENNEY, D. J. & MASLOWE, S. A. 1975 The evolution in space and time of nonlinear waves in parallel shear flows. *Stud. Appl. Maths* **54**, 181-205.

CRAIK, A. D. D. 1971 Non-linear resonant instability in boundary layers. *J. Fluid Mech.* **50**, 393-413.

GOLDSTEIN, M. E. 1983 The evolution of Tollmien–Schlichting waves near a leading edge. *J. Fluid Mech.* **127**, 59-81.

GOLDSTEIN, M. E. 1994 Nonlinear interactions between oblique instability waves on nearly parallel shear flows. *Phys. Fluids* **6**, 724-735.

GOLDSTEIN, M. E., DURBIN, P. A. & LEIB, S. J. 1987 Roll-up of vorticity in adverse-pressure-gradient boundary layers. *J. Fluid Mech.* **183**, 325-342.

GOLDSTEIN, M. E. & HULTGREN, L. S. 1988 Nonlinear spatial evolution of an externally excited instability wave in a free shear layer. *J. Fluid Mech.* **197**, 295-330.

GOLDSTEIN, M. E. & LEE, S. S. 1992 Fully coupled resonant-triad interaction in an adverse-pressure-gradient boundary layer. *J. Fluid Mech.* **245**, 523-551 (referred to herein as G&L).

GOLDSTEIN, M. E. & LEIB, S. J. 1988 Nonlinear roll-up of externally excited free shear layers. *J. Fluid Mech.* **191**, 481-515.

GRAEBEL, W. P. 1966 On determination of the characteristic equations for the stability of parallel flows. *J. Fluid Mech.* **24**, 497-508.

HULTGREN, L. S. 1992 Nonlinear spatial equilibration of an externally excited instability wave in a free shear layer. *J. Fluid Mech.* **236**, 635-664.

KACHANOV, YU. S. & LEVCHENKO, V. YA. 1984 The resonant interaction of disturbances at laminar–turbulent transition in a boundary layer. *J. Fluid Mech.* **138**, 209-247.

KLEBANOFF, P. S., TIDSTROM, K. D. & SARGENT, L. M. 1962 The three-dimensional nature of boundary layer instability. *J. Fluid Mech.* **12**, 1-34.

MANKBADI, R. R., WU, X. & LEE, S. S. 1993 A critical-layer analysis of the resonant triad in boundary-layer transition: nonlinear interactions. *J. Fluid Mech.* **256**, 85-106.

MASLOWE, S. A. 1986 Critical layers in shear flows. *Ann. Rev. Fluid Mech.* **18**, 405-432.

MILES, J. W. 1962 A note on the inviscid Orr–Sommerfeld equation. *J. Fluid Mech.* **13**, 427-432.

RAETZ, G. S. 1959 A new theory of the cause of transition in fluid flows. Northrop Corp. NOR-59-383 BLC-121.

REID, W. H. 1965 The stability of parallel flows. In *Basic Developments in Fluid Dynamics* (ed. M. Holt), Vol. 1, pp. 249-307. Academic.

WU, X. 1992 The nonlinear evolution of high-frequency resonant-triad waves in an oscillating Stokes layer at high Reynolds number. *J. Fluid Mech.* **245**, 553-597.